

# The QCD equation of state with dynamical quarks

---

**Szabolcs Borsányi<sup>a</sup>, Gergely Endrődi<sup>b</sup>, Zoltán Fodor<sup>a,b</sup>, Antal Jakovác<sup>a</sup>,  
Sándor D. Katz<sup>b</sup>, Stefan Krieg<sup>a,c</sup>, Claudia Ratti<sup>a</sup> and Kálmán K. Szabó<sup>a</sup>**

<sup>a</sup>*Department of Physics, University of Wuppertal, Gauss 20, D-42119, Germany*

<sup>b</sup>*Institute for Theoretical Physics, Eötvös University, Pázmány 1, H-1117 Budapest, Hungary*

<sup>c</sup>*Center for Theoretical Physics, MIT, Cambridge, MA 02139-4307, USA*

**ABSTRACT:** The present paper concludes our investigation on the QCD equation of state with 2+1 staggered flavors and one-link stout improvement. We extend our previous study [JHEP 0601:089 (2006)] by choosing even finer lattices. Lattices with  $N_t = 6, 8$  and 10 are used, and the continuum limit is approached by checking the results at  $N_t = 12$ . A Symanzik improved gauge and a stout-link improved staggered fermion action is utilized. We use physical quark masses, that is, for the lightest staggered pions and kaons we fix the  $m_\pi/f_K$  and  $m_K/f_K$  ratios to their experimental values. The pressure, the interaction measure, the energy and entropy density and the speed of sound are presented as functions of the temperature in the range  $100 \dots 1000$  MeV. We give estimates for the pion mass dependence and for the contribution of the charm quark. We compare our data to the equation of state obtained by the “hotQCD” collaboration.

**KEYWORDS:** Thermal Field Theory, Lattice QCD Thermodynamics.

---

## Contents

<b>1. Introduction</b>	<b>1</b>
<b>2. Methods</b>	<b>3</b>
2.1 Lattice discretization	4
2.2 Lines of constant physics	6
2.3 The integral technique	8
2.4 Hadron Resonance Gas Model	11
<b>3. Results</b>	<b>13</b>
<b>4. Conclusions, outlook</b>	<b>21</b>
<b>A. The pressure from a 2D spline fit</b>	<b>26</b>
<b>B. Tables</b>	<b>28</b>

---

## 1. Introduction

The study of QCD thermodynamics and that of the phase diagram are receiving increasing attention in recent years. A transition occurs in strongly interacting matter from a hadronic, confined system at small temperatures and densities to a phase dominated by colored degrees of freedom at large temperatures or densities. Lattice simulations indicate that the transition at vanishing chemical potential is merely an analytic crossover [1]. Even if strictly speaking there is no phase transition, it is common to use the words confined and deconfined phases for the low and high temperature regimes. This field of physics is particularly appealing because the deconfined phase of QCD can be produced in the laboratory, in the ultrarelativistic heavy ion collision experiments at CERN SPS, RHIC at Brookhaven National Laboratory, ALICE at the LHC and the future FAIR at the GSI. The close interplay between experimental data, numerical simulations on the lattice and phenomenological models offer the unique possibility of understanding the properties of matter under extreme conditions. The experimental results available so far show that the hot QCD matter produced experimentally exhibits robust collective flow phenomena, which are well and consistently described by near-ideal relativistic hydrodynamics [2, 3, 4]. These hydrodynamical models need as an input an Equation of State (EoS) which relates the local thermodynamic quantities. Therefore, an accurate determination of the QCD EoS is an essential ingredient to understand the nature of the matter created in heavy ion collisions, as well as to model the behavior of hot matter in the early universe.

Numerical simulations of QCD thermodynamics on the lattice are reaching unprecedented levels of accuracy, and a variety of data are now available for the EoS, including works in the quenched approximation [5, 6], two-flavor simulations [7, 8], studies with

heavier-than-physical [9, 10], and almost physical quark masses [11, 12, 13, 14]. In Reference [15], our collaboration has presented results for the EoS of 2+1 flavor QCD with physical quark masses, on lattices with temporal extensions  $N_t = 4$  and  $N_t = 6$  and for temperatures up to  $3T_c$ . Data for an EoS involving physical masses together with a careful continuum limit are so far missing; their relevance for the physics of the Quark-Gluon Plasma (QGP) is obvious.

An issue that is receiving increasing attention in recent years, is whether the charm quark can give an important contribution to the QCD EoS, in the range of temperatures which are reached in heavy ion collisions. It is often assumed that it can be neglected, the charm mass being too heavy to play any role at  $T \simeq 2 - 3T_c$ . However, perturbative QCD predicts that its contribution to thermodynamic observables is relevant at surprisingly low temperatures, down to  $T \simeq 350$  MeV [16]. Recent exploratory lattice studies have confirmed these expectations [17, 18], indicating a non-negligible contribution of the charm quark to thermodynamics already at  $1.2-2T_c$ . These results have been obtained on rather coarse lattices ( $N_t = 4, 6$ ) and with the charm quark treated in the quenched approximation.

Most of the available results on the QCD EoS have been obtained using improved staggered fermion actions. This formulation does not preserve the flavor symmetry of continuum QCD; as a consequence, the spectrum of low lying hadron states is distorted. Recent analyses performed by various collaborations [19, 20, 21] have pointed out that this distortion can have a dramatic impact on the thermodynamic quantities. In order to quantify this effect, one can compare the low temperature behavior of the observables obtained on the lattice, to the predictions of the Hadron Resonance Gas (HRG) model, and monitor how it reaches the continuum limit (for nonvanishing lattice spacings the spectrum is distorted, which has an influence on the prediction of the HRG model).

In this paper, we present our most recent results for several thermodynamic observables: pressure, energy density, entropy density, trace anomaly and speed of sound, for a system of  $n_f = 2 + 1$  flavors of dynamical quarks. We also determine the contribution of the charm quark to the pressure of the system. The charm quark is treated at the partially quenched level, i.e. we use the same gauge field configurations as in the  $n_f = 2 + 1$  case. We improve our previous findings [15] by choosing finer lattices ( $N_t = 8, 10$  and a few checkpoints at  $N_t = 12$ ). We work again with physical light and strange quark masses: we fix them by reproducing the physical ratios  $m_\pi/f_K$  and  $m_K/f_K$  for the lightest staggered tastes of these mesons and by this procedure [22] we get  $m_s/m_{u,d} = 28.15$ . Several values for the charm quark mass are used in the range  $m_c/m_s = 10.75 \dots 20$ . As we will see, the different sets of data corresponding to different  $N_t$  nicely agree with each other for all observables under study: for this reason, we expect that discretization effects are tiny. We also check that there are no significant finite size effects in the lattices that we use, by performing a set of simulations in a box with a size of 7 fm at the transition temperature. Our results are obtained in the range  $100 \text{ MeV} \lesssim T \lesssim 1000 \text{ MeV}$ . The simulations are performed by using the tree-level Symanzik improved gauge, and stout-improved staggered fermion action that we already used in [15]. Recently it has become clear [19, 20, 21] that the taste splitting due to the staggered formulation affects dramatically several thermodynamical observables at low temperatures. Together with the projected smeared links used in the recently proposed HISQ action [23, 24], the stout-smearing [25] has the smallest taste violation among the ones used so far in the literature for large scale thermodynamical simulations. Other staggered fermion actions with larger taste violation, such as the “asqtad”

and “p4fat” actions used by the “hotQCD” collaboration, suffer from these lattice artefacts more seriously. It is therefore not surprising that the results obtained in the present paper are rather different from the ones obtained by the “hotQCD” collaboration in Reference [14].

The paper is divided into two major parts: Section 2 describes the methods and techniques, which were used in this study. Those, who are interested in the results only, can skip this part and can go directly to Section 3, where we present and analyze our lattice results.

## 2. Methods

The fundamental quantity of finite temperature field theory is the partition function, any thermodynamic observable can be derived from it. After integrating out the quark fields ( $\psi_q$ , with flavor index  $q$ ) it can be written as a path integral over the gauge field  $U$ :

$$\mathcal{Z} = \int [dU] \exp(-\beta S_g(U)) \prod_q (\det M(U, m_q))^{1/4}. \quad (2.1)$$

Here  $S_g$  is the gauge action,  $\beta$  is related to the gauge coupling as  $\beta = 6/g^2$ , the staggered quark Dirac operator is  $M$  and  $m_q$  is the mass of the quark with flavor  $q$ . In this paper we use the same mass for the up and down flavors ( $m_{ud}$ ), the mass of the strange quark is denoted by  $m_s$  and the mass of the charm quark by  $m_c$ . The free energy density is  $f = -\frac{T}{V} \log \mathcal{Z}$ , where  $T$  denotes the temperature and  $V$  the three-volume of the system. In the thermodynamic limit the pressure is related to the free energy density as

$$p = - \lim_{V \rightarrow \infty} f. \quad (2.2)$$

In the following we will always assume to have a large enough, homogeneous system, so that the pressure can always be identified with the negative of the free energy. Later on we will check, that this condition can be safely assumed in case of the lattice simulations. Having calculated the pressure as a function of the temperature  $p(T)$ , all other thermodynamic observables can also be reconstructed. The trace anomaly  $I = \epsilon - 3p$  is a straightforward derivative of the normalized pressure:

$$I = T^5 \frac{\partial p(T)}{\partial T T^4} \quad (2.3)$$

Using the pressure and the trace anomaly the energy density  $\epsilon$ , the entropy density  $s$  and the speed of sound  $c_s$  can be calculated as

$$\epsilon = I + 3p, \quad s = \frac{\epsilon + p}{T}, \quad c_s^2 = \frac{dp}{d\epsilon}. \quad (2.4)$$

Next we will describe in detail the way we have calculated the thermodynamic observables in Equations (2.2), (2.3), (2.4) on the lattice. Our choice for the discretization of the gauge action and the quark Dirac operators and a discussion of the discretization effects is presented in Subsection 2.1. On the lattice, the gauge coupling and the quark masses are not independent, their relation is dubbed Lines of Constant Physics (LCP) and is described in Subsection 2.2. The pressure can be determined from lattice observables by an integral, this technique, with our specific improvements, is presented in Subsection 2.3. Finally we describe the HRG model in Subsection 2.4, which is used for comparison with the lattice calculations in the low temperature regime.

## 2.1 Lattice discretization

The compact Euclidean spacetime of temperature  $T$  and three-volume  $V$  is discretized on a hypercubic lattice with  $N_t$  and  $N_s$  points in the temporal and spatial directions:

$$T = \frac{1}{N_t a}, \quad V = (N_s a)^3, \quad (2.5)$$

where  $a$  is the lattice spacing. At a fixed  $N_t$ , the temperature can be set by varying the lattice spacing. This implies varying the bare parameters of the lattice action accordingly (see Subsection 2.2). At a fixed temperature, lattice discretization effects can be investigated by changing  $N_t$ , we used  $N_t = 6, 8, 10$  and  $12$  in this study. Finite volume effects were also studied by considering two different spatial volumes in the case of  $N_t = 6$ . For the renormalization we took lattices with  $N_t \geq N_s$ , at the present precision they can all be considered as having zero temperature. The following table summarizes the lattice sizes ( $N_t \times N_s^3$ ) and the temperature ranges of this study:

$N_t$	finite $T$	zero $T$	$T$ values
6	$6 \times 18^3, 6 \times 36^3$	$18 \times 18^3, 36 \times 18^3$	100 ... 1000 MeV
8	$8 \times 24^3$	$24 \times 24^3$	100 ... 1000 MeV
10	$10 \times 32^3$	$32 \times 32^3, 96 \times 32^3$	100 ... 365 MeV
12	$12 \times 32^3, 12 \times 64^3$	$32 \times 32^3, 64 \times 64^3$	132, 167, 223 MeV

In this work we use the same action as in our earlier studies on the QCD transition's order and characteristic temperatures [1, 15, 21, 22, 26]. As for the gauge field, it means a tree level Symanzik improvement. The fermions are discretized using the one-link staggered action with stout-smearred gauge links [25]. We employ two levels of the analytic smearing, each with the smearing parameter  $\rho = 0.15$ . In order to get rid of the unwanted doublers of the staggered formulation we use the ‘‘rooting procedure’’ [27].

The description of our updating algorithm can be also found in the above papers. The effectivity of these algorithms towards the continuum limit has been questioned recently [28], where a serious increase in the autocorrelation time of the topological charge was observed. On Figure 1 we show the Monte-Carlo time history of the topological charge in a zero temperature run on one of our finest lattice spacings ( $a = 0.054$  fm). The charge is measured by the naive operator after performing 30 HYP smearing steps on the gauge configurations. In our setup no dangerous critical slowing down can be observed. We have also looked for correlations between the topological charge and various thermodynamical observables. Those relevant for the equation of state show no significant dependence on the topological sectors.

In lattice field theory one attempts to reduce the cutoff effects by the so called improvement program. Not only the lattice action but also lattice observables can be improved. In lattice thermodynamics the cutoff effects depend on  $N_t$ , for  $N_t \rightarrow \infty$  they disappear. In our analysis we use a tree-level improvement for the pressure: we divide the lattice results with the appropriate improvement coefficients. These factors can be calculated analytically for our action and in case of the pressure we have the following values on different  $N_t$ 's:

$N_t = 6$	$N_t = 8$	$N_t = 10$	$N_t = 12$
1.517	1.283	1.159	1.099

We use the same factor for the two different spatial volumes in our finite volume study ( $6 \times 18^3$  and  $6 \times 36^3$ ). Using thermodynamical relations one can obtain these improvement

coefficients for the energy density, trace anomaly and entropy, too. The speed of sound receives no improvement factor at tree level. Note, that these improvement coefficients are exact only at tree-level, thus in the infinitely high temperature, non-interacting case. As we decrease the temperature, corrections to these improvement coefficients appear, which have the form  $1 + b_2(T)/N_t^2 + \dots$ . Empirically one finds that the  $b_2(T)$  coefficient, which describes the size of lattice artefacts of the tree-level improved quantities, is tiny not only at very high temperatures, but throughout the deconfined phase. In Section 3 we will present our findings for different lattice spacings on the effectivity of this improvement.

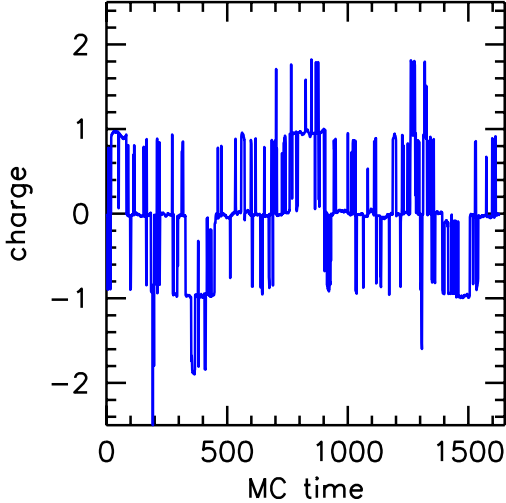


**Figure 1:** Monte-Carlo time history of the topological charge in a zero temperature run at  $a = 0.054$  fm lattice spacing.

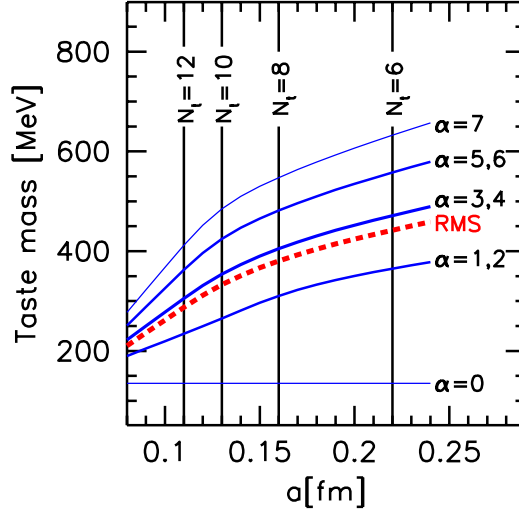


**Figure 2:** Masses of lattice pion tastes as the function of the lattice spacing. The different  $N_t$ 's correspond to  $T = 150$  MeV.

Taste symmetry breaking is a discretization error which is important mainly at low energies. In the staggered fermion formulation, hadron masses cannot be uniquely determined at any finite lattice spacing [29]. Each continuum hadron state has a corresponding multiplet of states on the lattice: due to the taste symmetry violation the masses of these states are split up. As an example, 16 lattice states correspond to each continuum pion state, each of them contributing with a  $1/16$  weight. The following table lists the members of the lattice pion multiplet with the taste structure (a  $4 \times 4$  complex matrix,  $\Gamma_\alpha$ ) and the multiplicity ( $n_\alpha$ ):

$\alpha$	0	1	2	3	4	5	6	7
$\Gamma_\alpha$	$\gamma_5$	$\gamma_0\gamma_5$	$\gamma_i\gamma_5$	$\gamma_i\gamma_j$	$\gamma_i\gamma_0$	$\gamma_i$	$\gamma_0$	1
$16 \cdot n_\alpha$	1	1	3	3	3	3	1	1

Only  $\alpha = 0$  behaves like a Goldstone-boson, i.e. its mass vanishes in the chiral limit. The other 15 states have masses of the order of several hundred MeVs for sensible values of the lattice spacing. Though these mass differences vanish in the continuum limit, it is very important to suppress them as much as possible. The effect of the heavier “pions” on the equation of state can be significant: they can reduce the QCD pressure and can also shift the transition temperature. Strategies for the suppression have been studied extensively. In general, using gauge link smearing in the fermion action proved to be a very efficient and cheap option. The mass splitting in the pion multiplet for our smearing recipe as a

function of the lattice spacing is shown on Figure 2. The pion state with the lowest mass is adjusted to the mass of the continuum pion. We plot the root mean squared (RMS) average of the masses with red dashed line. The four vertical lines correspond to lattice spacings on our four different  $N_t$ 's in the transition region (at  $T = 150$  MeV).

## 2.2 Lines of constant physics

On a lattice with fixed  $N_t$  we change the temperature by changing the lattice spacing. This can be achieved by varying the bare parameters of the action:  $\beta$  and the quark masses. The fact that towards the continuum limit the lattice should reproduce the continuum physics, dictates the functional relation between these parameters. Our LCP was defined so, that the mass and decay constant of the lightest staggered kaon and the mass of the lightest staggered pion are related to each other as the corresponding continuum values<sup>1</sup>. This then translated to a quark mass ratio  $m_s/m_{ud} = 28.15(1)$  and to the functions  $m_s^{\text{phys}}(\beta)$  and  $a(\beta)$  (see upper part of Table 1). When we say that quark masses are set to their physical values, we mean that they are on this LCP ( $m_{ud}^{\text{phys}}(\beta)$  and  $m_s^{\text{phys}}(\beta)$ ). For details see References [22, 26], where the LCP was determined in the range  $\beta = 3.45 \dots 3.85$ . In the following, we refer to this technique as our “old method”.

In this work we determine the LCP up to  $\beta \approx 4.62$ , which allows us to calculate thermodynamical observables up to temperatures as high as  $\sim 1$  GeV. Due to the smallness of the lattice spacing at these  $\beta$  values, the calculation of hadronic observables is impossible with the present computer resources. Thus the conventional way (our “old method”) to determine the LCP by measuring ratios of hadronic observables fails here. We circumvented the problem by applying an iterative procedure analogous to the well-known step scaling technique [31]. In order to simplify the discussion, first we introduce the technique without quarks, ie. in the pure gauge case. The inclusion of quarks will be described afterwards. Later on we refer to this technique as our “new method”.

We make simulations on symmetric lattices ( $N^4$ ) with  $N \leq 24$ . For small lattice spacings they are in the “deconfined phase”, no hadronic observable can be used for scale setting here. Therefore we use the Creutz ratio ( $\chi$ ) for the scale setting similarly to what was proposed in [32]. On a  $N^4$  lattice at coupling  $\beta$  we define an effective coupling by measuring symmetric Creutz ratios<sup>2</sup> of size  $N/4$ :

$$g_{\text{eff}}^2(N, \beta) = N^2 \chi(N/4). \quad (2.6)$$

Let us assume, that we have already determined the LCP, in this case a single  $\beta(a)$  function, for lattice spacings larger than  $a_0$ . This is obtained by fixing some observables in the

a [fm]	$\beta$	$m_s^{\text{phys}}(\beta)$
0.2824(6)	3.45	$1.57 \cdot 10^{-1}$
0.2173(4)	3.55	$1.02 \cdot 10^{-1}$
0.1535(3)	3.67	$6.39 \cdot 10^{-2}$
0.1249(3)	3.75	$5.03 \cdot 10^{-2}$
0.0989(2)	3.85	$3.94 \cdot 10^{-2}$
0.0824	3.938(3)	$3.30 \cdot 10^{-2}$
0.0687	4.036(5)	$2.71 \cdot 10^{-2}$
0.0572	4.140(6)	$2.24 \cdot 10^{-2}$
0.0477	4.255(8)	$1.88 \cdot 10^{-2}$
0.0397	4.360(12)	$1.59 \cdot 10^{-2}$
0.0331	4.486(11)	$1.31 \cdot 10^{-2}$
0.0276	4.615(9)	$1.04 \cdot 10^{-4}$

**Table 1:** The line of constant physics used in this work. The upper half of this table quotes the figures of Reference [22], the lower half is the result of our iterative scheme. For  $a$ ,  $m_s^{\text{phys}}$  we estimate the systematic errors to be 2%.

<sup>1</sup>We take  $f_K = 155.5$  MeV,  $m_\pi = 135$  MeV and  $m_K = 495$  MeV from the Particle Data Group [30].

<sup>2</sup>We use APE smearing to enhance the signal/noise ratio [33].

hadronic phase (e.g.  $r_0$  or glueball mass). Now we want to determine this function for a lattice spacing smaller than  $a_0$ . We take lattices of size  $12^4$ ,  $16^4$  and  $20^4$  with different lattice spacings, so that the size of the lattices in physical units is to be the same, which is at couplings  $\beta(20/12 \cdot a_0)$ ,  $\beta(20/16 \cdot a_0)$ ,  $\beta(20/20 \cdot a_0)$ . Then we make a continuum extrapolation from the measured effective couplings to  $a_1 = 20/24 \cdot a_0 < a_0$  and search for the  $\beta$  parameter at which the  $g_{\text{eff}}^2$  is reproduced on a  $24^4$  lattice. This defines  $\beta(a_1)$  and completes one step of iteration. The next iteration repeats the above steps using  $a_1$  instead of  $a_0$ . Thus, one receives a series of  $\beta$  values, which correspond to smaller and smaller lattice spacings:  $a_{i+1} = 20/24 \cdot a_i$ .

As a test, we used this method to determine the  $\beta(a)$  function in the pure gauge case using the plaquette gauge action. We initialized the first iteration with  $\beta < 6.0$  data. For comparison, we take the simulations up to  $\beta < 6.92$  from [34] and an extrapolation based on the results of [35]. The agreement is maintained over more than an order of magnitude in the lattice spacing (see Figure 3).

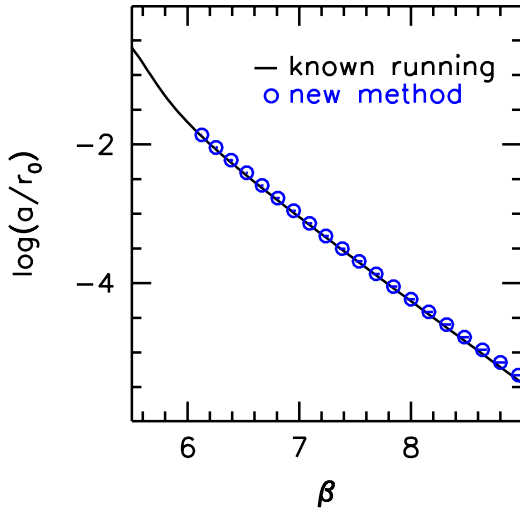


**Figure 3:** Lattice spacing as a function of  $\beta$  in the pure gauge case using the Wilson action. The points are obtained with our variant of the step scaling method, the line is the already known running.

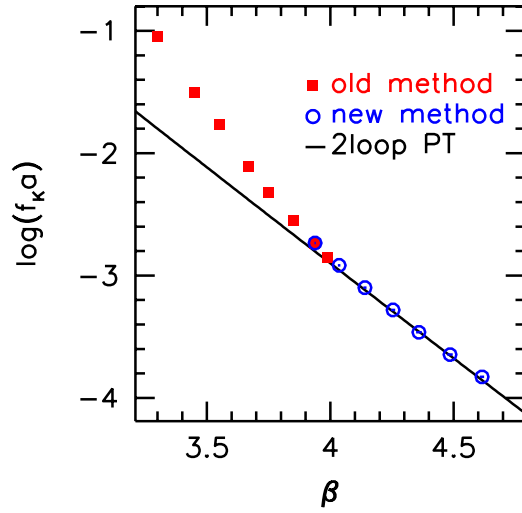


**Figure 4:** Lattice spacing as a function of  $\beta$  in the dynamical  $n_f = 2 + 1$  case for our action. The blue circles are obtained with our new method, the red squares with the old one by measuring hadronic observables. The black curve is the 2-loop perturbative running.

If one would like to include the quarks properly, a renormalized observable, that is not related to the hadronic scale and is sensitive to the quark masses would be necessary. The above iterative procedure then would have to be generalized, where not only the  $\beta$  but the quark masses would have to be tuned. Since we know, that for small enough lattice spacings the running of the scale does not depend on the quark masses and that for high temperatures the thermodynamics shows a very small quark mass dependence, the quark masses can be determined with less precision. Therefore from  $\beta > 3.94$  we have abandoned this multi-parameter tuning and simply used the 1-loop running of the quark mass in the



simulations<sup>3</sup>. The obtained results are tabulated in the lower part of Table 1. Since the new method measures the  $\beta$  at a given lattice spacing, the errors are attributed to the  $\beta$  values. The running of the coupling is shown on Figure 4. Note, that we have an overlap between the lattice spacings obtained by the “old” and the “new” methods. Together with the simulation points with these techniques, we also show the two-loop perturbative running. A satisfactory agreement is found for  $\beta > 4.1$ .

At  $\beta = 3.99$  we have checked the resulting LCP using a zero temperature simulation with physical quarks on a  $64^4$  lattice. On Figure 4 the highest  $\beta$  point with the old method corresponds to this simulation. Setting the scale by  $f_K$  we get results compatible with the physical hadron spectrum:

$m_\pi$	$m_K$	$m_{\eta_s}$	$f_\pi$
134.2(6) MeV	497.7(6) MeV	690(4) MeV	131.0(7) MeV

whereas for the lattice spacing we find  $a = 0.0735(4)$  fm. These results justify the correctness of our new technique to determine the LCP. In the range  $\beta = 3.85 \dots 4.1$  we also performed control simulations in smaller volumes (with  $N \approx 2$  fm). These showed up to 2% deviations from the line of constant physics determined with the new method. This gives an estimate of the systematic errors coming from scale setting used in this work.

We also study the thermodynamics of QCD for heavier than physical quark masses. The corresponding renormalized trajectories are defined by setting the strange mass to the above obtained  $m_s^{\text{phys}}(\beta)$ , whereas the light quark mass is set to  $m_{ud}(\beta) = m_s^{\text{phys}}(\beta)/R$ , where the quark mass ratio  $R$  is varied in the range  $R = 1 \dots 28.15$ . Since these are hypothetical theories with nonphysical quark masses, strictly speaking they are not related to scales in physical units (e.g. fm). Nevertheless, it is useful to use physical scales also in this case. To this end, for heavier than physical quark masses we use the standard mass independent scale setting, thus  $\beta(a)$  is the same as for physical quark masses.

Furthermore, we also give an estimate for the contribution of the charm quark to thermodynamics. The charm quark mass is not very well known experimentally, whereas there is a recent high precision lattice calculation of the charm to strange mass ratio [36]. We denote this ratio by  $Q = m_c/m_s$  and the recent lattice estimate is  $Q = 11.85(16)$ . In addition to the central value of this lattice result, we carried out the analysis for several other values in the range  $Q = 10.75 \dots 20$ . The effect of the charm was determined at the partially quenched level, ie. its back-effects on the gauge background were neglected. We leave it for future work to include the charm quark dynamically.

### 2.3 The integral technique

In order to fix the notations we first quickly review the standard method, which is used to determine the equation of state (“integral technique”, [37]). On the lattice, the dimensionless pressure

$$p^{\text{lat}}(\beta, m_q) = (N_t N_s^3)^{-1} \log \mathcal{Z}(\beta, m_q) \quad (2.7)$$

is in itself not accessible using conventional algorithms, only its derivatives with respect to the bare parameters of the action are measurable. Using these partial derivatives the

---

<sup>3</sup>The running of the quark mass in the range  $\beta = 3.85 \dots 3.94$  was determined by tuning the  $\beta$  and the quark masses and monitoring the pseudoscalar meson masses.

pressure can be rewritten as a multidimensional integral along a path in the space of bare parameters:

$$p^{\text{lat}}(\beta, m_q) - p^{\text{lat}}(\beta_0, m_{q0}) = (N_t N_s^3)^{-1} \int_{(\beta_0, m_{q0})}^{(\beta, m_q)} \left( d\beta \frac{\partial \log \mathcal{Z}}{\partial \beta} + \sum_q dm_q \frac{\partial \log \mathcal{Z}}{\partial m_q} \right), \quad (2.8)$$

where we used the index ‘0’ to denote the starting point of the integration. The value of the pressure at parameters ‘0’ has to be handled with care: one either chooses the starting point so deeply in the strong coupling regime, so that the  $p^{\text{lat}}(\beta_0, m_{q0})$  can already be neglected or it can be taken from model computations (see Subsection 2.4). The derivatives in this formula are the gauge action and the chiral condensate densities:

$$\langle -s_g \rangle = (N_t N_s^3)^{-1} \frac{\partial \log \mathcal{Z}}{\partial \beta}, \quad \langle \bar{\psi}_q \psi_q \rangle = (N_t N_s^3)^{-1} \frac{\partial \log \mathcal{Z}}{\partial m_q}. \quad (2.9)$$

The pressure itself contains additive divergences, which are independent of the temperature. Removing them can be done by subtracting the same observables measured on a lattice, with the same bare parameters but at a different temperature value, ie. with a different temporal extent  $N_t^{\text{sub}}$ . Here we use lattices with a large enough temporal extent, so it can be regarded to have zero temperature. These are denoted as “zero  $T$ ” lattices in Subsection 2.1. The finiteness of  $N_t^{\text{sub}}$  causes an error of the order  $(N_t/N_t^{\text{sub}})^4$ , which is smaller than the typical size of the statistical error. Using the subtracted observables

$$\langle s_g \rangle^{\text{sub}} = \langle s_g \rangle_{N_t, N_s} - \langle s_g \rangle_{N_t^{\text{sub}}, N_s} \quad (2.10)$$

$$\langle \bar{\psi}_q \psi_q \rangle^{\text{sub}} = \langle \bar{\psi}_q \psi_q \rangle_{N_t, N_s} - \langle \bar{\psi}_q \psi_q \rangle_{N_t^{\text{sub}}, N_s} \quad (2.11)$$

one can express the renormalized pressure as:

$$\frac{p(T)}{T^4} - \frac{p(T_0)}{T_0^4} = N_t^4 \int_{(\beta_0, m_{q0})}^{(\beta, m_q)} \left( d\beta \langle -s_g \rangle^{\text{sub}} + \sum_q dm_q \langle \bar{\psi}_q \psi_q \rangle^{\text{sub}} \right), \quad (2.12)$$

where we have normalized it by  $T^4$  as usual. The  $T$  and  $T_0$  are the temperature values corresponding to the lattice spacing at the bare parameters  $(\beta, m_q)$  and  $(\beta_0, m_{q0})$ . Using Equation (2.3) one can also relate the integrand to the trace anomaly:

$$\frac{I(T)}{T^4} \frac{dT}{T} = N_t^4 \left( d\beta \langle -s_g \rangle^{\text{sub}} + \sum_q dm_q \langle \bar{\psi}_q \psi_q \rangle^{\text{sub}} \right). \quad (2.13)$$

Let us make an observation here: due to the  $N_t^4$  prefactor in the trace anomaly the subtracted observables decrease with the lattice spacing (at a fixed temperature this means an increasing  $N_t$ ). While  $\langle -s_g \rangle^{\text{sub}}$  decreases as  $N_t^{-4}$ , the chiral condensate behaves substantially different. Due to chiral symmetry<sup>4</sup>  $\langle \bar{\psi}_q \psi_q \rangle$  is proportional to the bare quark mass, moreover it is also multiplied by another power of the bare quark mass ( $dm_q$  line-element) in the trace anomaly. Since the bare mass also decreases with the lattice spacing, the subtracted condensate only decreases as  $N_t^{-2}$ . These scalings are directly translated into different precisions for the two terms in Equation (2.13). The term with the gauge action

---

<sup>4</sup>Staggered fermions have only a remnant chiral symmetry, but this does not affect the argument.

density has  $N_t^2$  times larger errors than the term with the chiral condensate, if they are evaluated with the same statistics.

The standard integral method proceeds as follows: first one calculates the trace anomaly for several temperatures along the lines of constant physics and then integrates it to get the pressure up to an integration constant (which can be either neglected or taken from a model calculation). This path was used in several lattice studies, e.g. [12, 13, 14, 15].

One of our major goals with this paper is to determine the equation of state for several (heavier than physical) different values of the light quark masses. We therefore carried out simulations covering an extended region in the  $\{\beta, m_s, m_{ud}\}$  parameter space. The strange mass  $m_s$  was always set to its physical value  $m_s^{\text{phys}}(\beta)$  and  $m_{ud}$  was set as  $m_{ud}(\beta) = m_s(\beta)/R$  with the quark mass ratio  $R$  ranging from 1 to  $R^{\text{phys}} = 28.15$ . The value  $R = 1$  corresponds to the three degenerate flavor case, whereas  $R^{\text{phys}}$  is the “real world” value of the quark mass ratio. At these parameters we can consider the pressure as a function of only two variables:  $\beta$  and  $R$ . The respective derivatives can be measured on the lattice, they are given by the following formulas:

$$D_\beta = \frac{\partial}{\partial \beta} \bigg|_R \frac{p(T)}{T^4} = N_t^4 \left[ \langle -s_g \rangle^{\text{sub}} + \frac{\partial m_s^{\text{phys}}}{\partial \beta} (\langle \bar{\psi}_s \psi_s \rangle^{\text{sub}} + \frac{1}{R} \langle \bar{\psi}_{ud} \psi_{ud} \rangle^{\text{sub}}) \right], \quad (2.14)$$

$$D_R = \frac{\partial}{\partial R} \bigg|_\beta \frac{p(T)}{T^4} = -N_t^4 \frac{m_s^{\text{phys}}}{R^2} \langle \bar{\psi}_{ud} \psi_{ud} \rangle^{\text{sub}}. \quad (2.15)$$

These derivatives have to be integrated to obtain the pressure. Since the integrand is in itself a total derivative, the result is independent of the chosen integration path in the two dimensional space of the parameters  $\beta$  and  $R$  (see Figure 5 for an illustration). The simulation points are denoted by crosses. The straightforward way would be to perform a one dimensional integral in  $\beta$  at a fixed value of the quark mass ratio  $R$ , this corresponds to path A. However one can also imagine zigzagging routes, like path B or C on the Figure. Averaging several of such integrals, one can increase statistics and it also provides an estimate of the systematic error related to the integration path.

Here we propose a generalized method that takes into account every possible integration path at the same time. The main idea is – instead of parametrizing the derivatives of the pressure and then integrate – to parametrize the pressure itself. A straightforward parametrization is one using the actual values  $p_{kl}$  of the pressure at some node points  $\{\beta_k, R_l\}$  that build up a two-dimensional spline function – i.e. that unambiguously determine the whole pressure surface as a function of  $\beta$  and  $R$ . The parameters  $p_{kl}$  can be set to minimize the deviation between the derivatives of this surface and the measured values  $D_\beta$  and  $D_R$ . This minimum condition leads to a system of linear equations that can be solved for  $p_{kl}$ . This method gives the pressure directly using the information contained in the derivatives  $D_\beta$  and  $D_R$  without the need to carry out an actual integration. The details of this analysis can be found in Appendix A and in Reference [38], where the systematic error of the method is also discussed.

The method determines the pressure only up to an overall constant factor, which corresponds to an integration constant and originates from the fact that the derivatives  $D_\beta$  and  $D_R$  are measured at finite values of the temperature. We set this constant, so that at the smallest temperature for three degenerate flavors the pressure is set to zero:

$$p(T = 100\text{MeV}, R = 1) = 0. \quad (2.16)$$

The error of this choice is hard to estimate from the lattice alone. It is definitely more reasonable to set the zero here, than at the physical point  $R = R^{\text{phys}}$ , since the hadrons are much heavier here and therefore their contribution to the pressure is smaller. According to the HRG model (see Subsection 2.4) the pressure at this point  $p^{\text{HRG}}(T)/T^4 = 0.02$  is much smaller than the typical statistical errors on the lattice.

Starting from the above obtained parametrization of the pressure we derived the trace anomaly using Equation (2.3). In order to be able to give smooth curves as results, we fitted the trace anomaly with a 4-degree spline function. In this way the smoothness of the further derived quantities ( $\epsilon$ ,  $s$  and  $c_s$ ) was ensured, too. The variation of the nodepoints of this spline interpolation was used to estimate the systematic error.

The above described method was used to determine the equation of state on  $N_t = 6, 8$  lattices for different values of the quark masses. In the case of  $N_t = 10$  we determined the equation of state exclusively with physical quark masses. In order to satisfy the normalization condition in Equation (2.16), we made heavier mass simulations at  $T = 100$  MeV up to the three flavor point. On  $N_t = 12$  we made simulations at three temperature values, this allows us to calculate the trace anomaly only.

For  $N_t = 8$  we also estimated the size of the contribution of the charm quark. In order to obtain this contribution, the  $\beta$  derivative of the pressure in Equation (2.14) has to be modified by adding the charm condensate:

$$D_\beta \rightarrow D_\beta + \frac{\partial m_s}{\partial \beta} \cdot Q \cdot \langle \bar{\psi}_c \psi_c \rangle^{\text{sub}}. \quad (2.17)$$

Let us emphasize it here again, that we use the partially quenched approximation, when calculating the observables in the  $n_f = 2 + 1 + 1$  theory: we neglect the back effect of charm quarks on the gauge fields.

## 2.4 Hadron Resonance Gas Model

The Hadron Resonance Gas model has been widely used to study the hadronic phase of QCD in comparison with lattice data [39, 40, 41]. The low temperature phase is dominated by pions. Goldstone's theorem implies weak interactions between pions at low energies, which allows to study them within Chiral Perturbation Theory ( $\chi$ PT) [42]. As the temperature  $T$  increases, heavier states become more relevant and need to be taken into account. The HRG model has its roots in the theorem by Dashen, Ma and Bernstein [43], which allows to calculate the microcanonical partition function of an interacting system, in the thermodynamic limit  $V \rightarrow \infty$ , to a good approximation, assuming that it is a gas of non-interacting free hadrons and resonances [44].

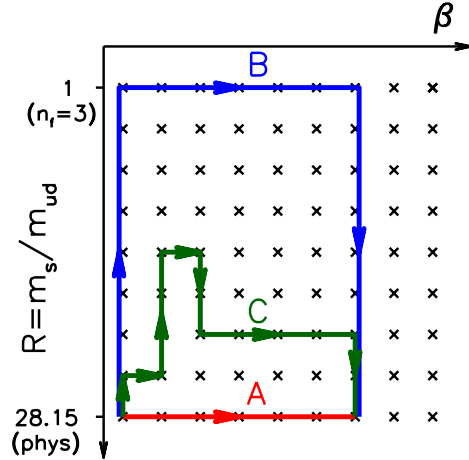


**Figure 5:** Illustration of possible integration paths, which can be used to obtain the pressure at a certain point. For explanation see the text.

The pressure of the HRG model can be written as the sum of independent contributions coming from non-interacting resonances

$$\frac{p^{\text{HRG}}}{T^4} = \frac{1}{VT^3} \sum_{i \in \text{mesons}} \log \mathcal{Z}^M(T, V, \mu_{X^a}, m_i) + \frac{1}{VT^3} \sum_{i \in \text{baryons}} \log \mathcal{Z}^B(T, V, \mu_{X^a}, m_i), \quad (2.18)$$

where

$$\begin{aligned} \log \mathcal{Z}^M(T, V, \mu_{X^a}, m_i) &= -\frac{Vd_i}{2\pi^2} \int_0^\infty dk k^2 \log(1 - z_i e^{-\varepsilon_i/T}), \\ \log \mathcal{Z}^B(T, V, \mu_{X^a}, m_i) &= \frac{Vd_i}{2\pi^2} \int_0^\infty dk k^2 \log(1 + z_i e^{-\varepsilon_i/T}), \end{aligned} \quad (2.19)$$

with energies  $\varepsilon_i = \sqrt{k^2 + m_i^2}$ , degeneracy factors  $d_i$  and fugacities

$$z_i = \exp\left(\left(\sum_a X_i^a \mu_{X^a}\right)/T\right). \quad (2.20)$$

In the above equation,  $X^a$  are all possible conserved charges, including the baryon number  $B$ , electric charge  $Q$  and strangeness  $S$ . The sums in Equation (2.18) include all known baryons and mesons up to 2.5 GeV, as listed in the latest edition of the Particle Data Book [30]. Notice, that only a few resonant states with masses larger than 2 GeV have been identified and got into the listing of the Particle Data Group. Attempts to improve the HRG model by including an exponential mass spectrum for these heavy resonances have been proposed [45, 46, 47]. In the present analysis we will consider only the known states and not include this exponential spectrum.

For temperatures  $T \lesssim 60\text{-}100$  MeV the contribution of the pions dominate the pressure, for larger temperatures, the kaon contribution becomes also sizable. Heavier states become relevant for  $T \gtrsim 120$  MeV.

As we have already discussed in Subsection 2.1 the staggered lattice discretization has a considerable impact on the hadron spectrum. In order to investigate these errors, we define a ‘‘lattice HRG’’ model, where in the hadron masses lattice discretization effects are taken into account. We consider only the taste splitting effects for the pions and the kaons. For example the contribution of the pions to the normalized pressure is now given by a sum, which runs over the different pion tastes:

$$\frac{1}{VT^3} \sum_{\alpha=0}^7 n_\alpha \log \mathcal{Z}^M(T, V, \mu_{X^a}, m_\alpha), \quad (2.21)$$

where the  $n_\alpha$  multiplicities are taken from the table in Subsection 2.1, the  $m_\alpha$  masses are those of the different pion tastes taken from the lattice simulations.

On Figure 6 we plot the normalized trace anomaly of the HRG model with the physical and with the lattice distorted spectrum for the four different lattice temporal extensions used in our investigations. The difference between the physical and lattice curves is a first estimate of the lattice discretization errors arising from the taste violation. As the temperature decreases at a fixed  $N_t$ , the lattice spacing gets larger and so do the taste violation effects. The model calculation suggests, that the lattice results may have sizeable

systematic errors in the low temperature region. Above  $T \sim 100$  MeV, this error estimate for the interaction measure is smaller than the typical magnitude of other errors in lattice QCD calculations. The overall uncertainties related to the above phenomenon will be discussed later.

In order to compare the HRG model results with our additional lattice simulations at larger-than-physical quark masses, we need the pion mass dependence of all hadrons and resonances included in the calculation. As we already did in [21], we assume that all resonances behave as their fundamental state hadrons as functions of the pion mass. For the fundamental hadrons, we use the pion mass dependence from Reference [19]. For larger-than-physical quark masses, the taste symmetry violation at finite lattice spacing has a milder impact on the pressure. This also motivates to take  $R = 1$  as the starting point of the integration of the pressure at  $T = 100$  MeV (see Subsection 2.3).

### 3. Results

In this section we present our results on the equation of state. First we discuss finite volume effects and discretization artefacts. Then we show the  $n_f = 2 + 1$  flavor pressure, the interaction measure, the energy and entropy density as well as the speed of sound. We identify characteristic points in the temperature dependence of these observables and we also provide a parametrization. Moreover, we discuss the mass dependence of the equation of state. Afterwards we determine the size of the contribution of the charm quark within the partially quenched framework. Finally we compare our results to the existing literature.

For high temperatures the thermodynamic quantities approach the values of the non-interacting massless relativistic gas, the so-called Stefan-Boltzmann limit. The limit for the three flavor pressure is  $p_{SB}/T^4 \approx 5.209$ , for the energy density  $\epsilon_{SB} = 3p_{SB}$  and for the entropy density  $s_{SB} = 4p_{SB}/T$ .

The error bars on the figures are obtained by quadratically adding the statistical error and the systematic error of the integral method (Subsection 2.3). If no error bar is shown on a point, then the errorbar is smaller than the pointsize. The temperature values have an error at the 2% level arising from the scale setting procedure (Subsection 2.2).

#### Finite volume and discretization effects

In order to verify that there are no significant finite size effects present in the lattice data with the aspect ratio  $N_s/N_t = 3$ , we checked our  $N_t = 6$  data against a set of high precision  $N_s/N_t = 6$  simulations. The latter lattice geometry corresponds to about 7 fm box size at the transition temperature. Figure 7 shows the comparison between the two volumes for the normalized trace anomaly  $I/T^4$ . From this result we concluded that it is acceptable

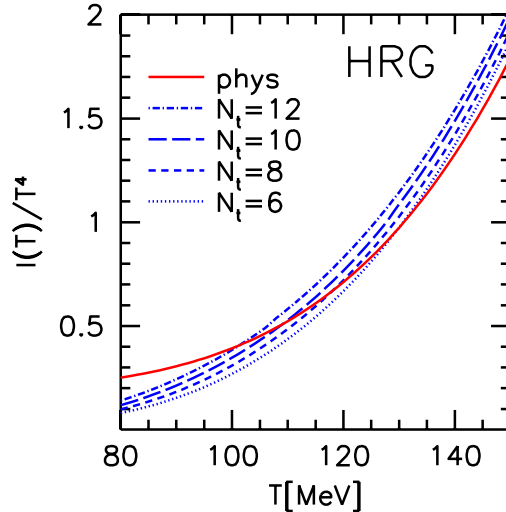


**Figure 6:** The normalized trace anomaly in the physical HRG model (solid red line) and in the HRG models with the lattice hadron spectrum (dashed blue lines).

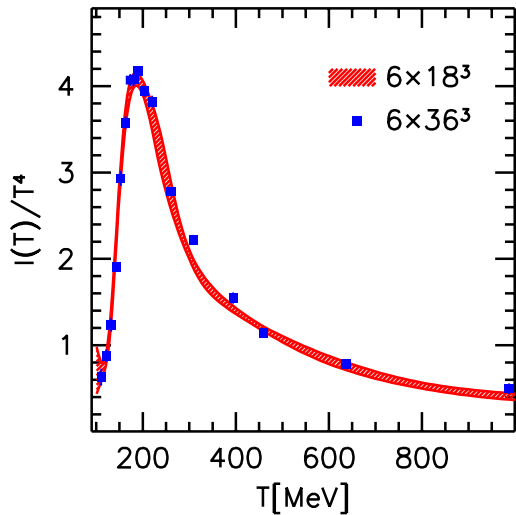


**Figure 7:** The trace anomaly on lattices with different spatial volumes:  $N_s/N_t = 3$  (red band) and  $N_s/N_t = 6$  (blue points).

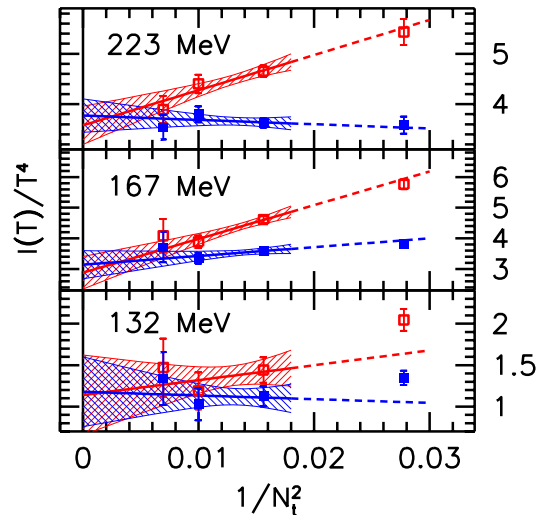


**Figure 8:** The trace anomaly at three different temperatures as a function of  $1/N_t^2$ . Filled blue symbols represent the results within the lattice tree-level improvement framework, red opened symbols show the results without this improvement. The error of the continuum extrapolated value is about 0.4 for all three temperatures.

to perform the more expensive simulations throughout with  $N_s/N_t = 3$ . Note, however, that for small temperatures this analysis on  $N_t = 6$  might underestimate the finite volume effects on finer lattices, since due to lattice artefacts many of the staggered pion states are very heavy. Let us also note here, that the volume independence in the transition region is an unambiguous evidence for the crossover type of the transition.

In order to decrease lattice artefacts, we apply the tree-level improvement for our thermodynamic observables (see Subsection 2.1). Figure 8 illustrates at three temperature values ( $T = 132, 167$  and  $223$  MeV) the effectiveness of this improvement procedure. We show both the unimproved and the improved values of the trace anomaly for  $N_t = 6, 8, 10$  and  $12$  as a function of  $1/N_t^2$ . The lines are linear continuum extrapolations using the three smallest lattice spacings. As it can be seen in the continuum limit both the unimproved and the improved observables converge to the same value. The figure confirms the expectations, that lattice tree-level improvement effectively reduces the cutoff effects. At all three temperatures the unimproved observables have larger cutoff effects than the improved ones. Actually, all the three values of  $b_2(T)$ , which indicate the remaining cutoff effects after tree-level improvement (see Subsection 2.1), differ from zero with less than one standard deviation.

### The $n_f = 2 + 1$ flavor equation of state

On Figure 9 we show the trace anomaly of QCD with  $n_f = 2 + 1$  flavor dynamical quarks as a function of the temperature. We have results at four different lattice spacings. As it can be seen on the figure, our results show essentially no dependence on the lattice spacing, they all lie on top of each other. Only the coarsest  $N_t = 6$  lattice shows some deviations around

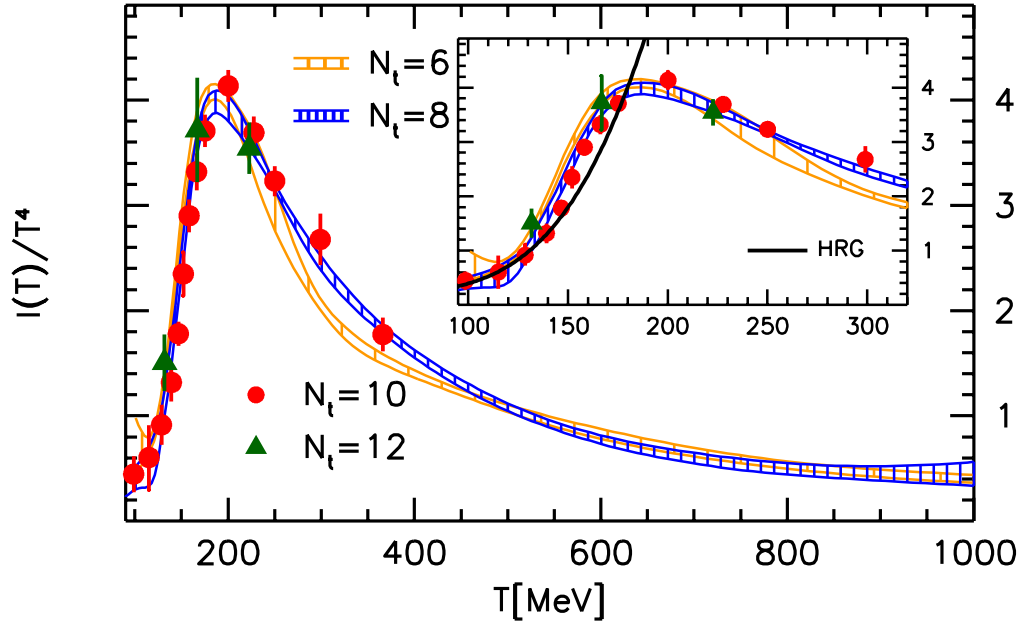


**Figure 9:** The trace anomaly  $I = \epsilon - 3p$  normalized by  $T^4$  as a function of the temperature on  $N_t = 6, 8, 10$  and  $12$  lattices.

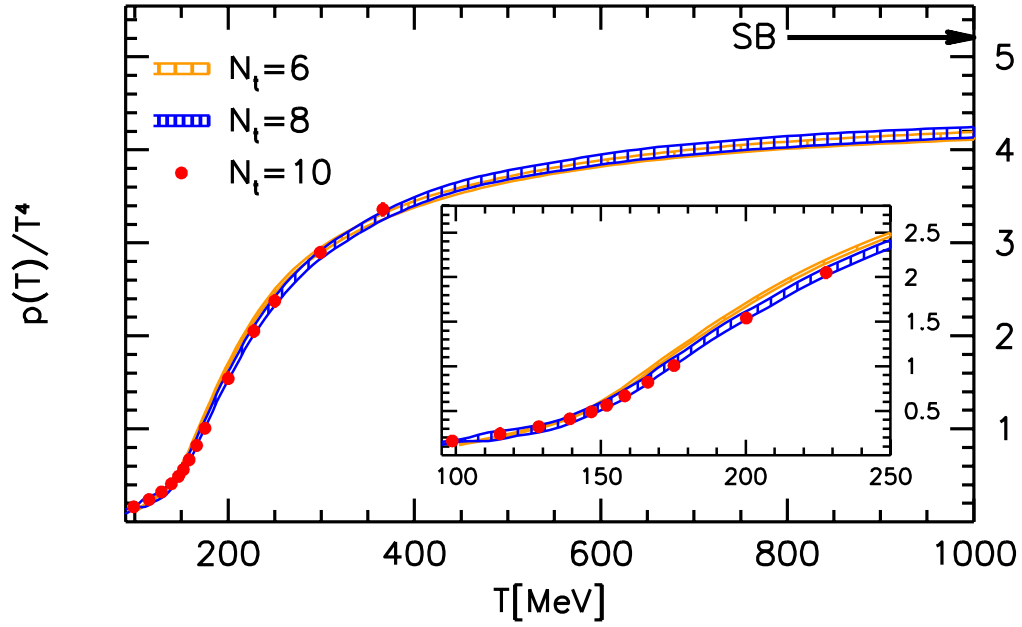


**Figure 10:** The pressure normalized by  $T^4$  as a function of the temperature on  $N_t = 6, 8$  and  $10$  lattices. The Stefan-Boltzmann limit  $p_{SB}(T) \approx 5.209 \cdot T^4$  is indicated by an arrow. For our highest temperature  $T = 1000$  MeV the pressure is almost 20% below this limit.



$\sim 300$  MeV. On the same figure, we also provide a zoom of the transition region. Here we also show the results from the HRG model: a good agreement with the lattice results is found up to  $T \sim 140$  MeV. One characteristic temperature of the crossover transition can be defined as the inflection point of the trace anomaly. This and other characteristic features of the trace anomaly are the following:

Inflection point of $I(T)/T^4$	152(4) MeV
Maximum value of $I(T)/T^4$	4.1(1)
$T$ at the maximum of $I(T)/T^4$	191(5) MeV

On Figure 10 we show the main result of our paper: the pressure of QCD with  $n_f = 2+1$  flavor dynamical quarks as a function of the temperature. We have results at three different lattice spacings. The  $N_t = 6$  and  $N_t = 8$  are in the temperature range from 100 up to 1000 MeV. The results on  $N_t = 10$  are in the range from 100 up to 365 MeV. As we have already discussed in Subsection 2.3, the zero point of the pressure is set by Equation (2.16). From this condition we get a nonzero pressure even at our smallest temperature  $T = 100$  MeV, when the physical values of the quark masses are used. This value is approximately two third of the value suggested by the HRG model. The origin of this difference cannot be clarified at the moment. One expects that the lattice artefacts are considerably larger at low temperatures, than what one estimates from the difference of  $N_t = 6, 8$  and 10 results. This is quite reasonable, since even our finest lattice at  $T = 100$  MeV has  $\sim 0.2$  fm lattice spacing, which is far from the regime, where lattice results starts to scale. On the other hand, this discrepancy might point to the failure of the HRG model. In order to be on the safe side we consider the size of this unexplained difference as an estimate of our systematic uncertainty in the low temperature regime.

On Figures 11 and 12 we show the energy density and the entropy density, on Figures 13 and 14 the speed of sound and  $p/\epsilon$  are shown. On the latter we plot the quantities as functions of the energy density. One can also read off the characteristic points of these curves, for convenience we tabulate the results here:

Minimum value of $c_s^2(T)$	0.133(5)
$T$ at the minimum of $c_s^2(T)$	145(5) MeV
$\epsilon$ at the minimum of $c_s^2(T)$	0.20(4) GeV/fm <sup>3</sup>
Minimum value of $p/\epsilon$	0.145(4)
$T$ at the minimum of $p/\epsilon$	159(5) MeV
$\epsilon$ at the minimum of $p/\epsilon$	0.44(5) GeV/fm <sup>3</sup>

In Appendix B we tabulate the pressure, the trace anomaly and the speed of sound for the  $N_t = 6, 8$  and 10 lattices. We also provide a continuum estimate<sup>5</sup> for these quantities: we take the average of the data at the smallest two lattice spacings and as an error we assign either the half-difference of the two or the statistical error depending on whichever is larger. As we have already explained, for low temperatures the lattice result for the pressure is significantly smaller than the prediction of the HRG model: at  $T = 100$  MeV the lattice result is  $p(T)/T^4 = 0.16(4)$ , whereas the model prediction is  $p(T)/T^4 = 0.27$ . Therefore in the continuum estimate of the pressure we shift the central values of the lattice results up by the half of this difference (0.06) and this shift is then considered as a systematic error in the entire temperature range.

<sup>5</sup>For a rigorous continuum extrapolation one would need  $N_t = 12$  for the entire temperature region.

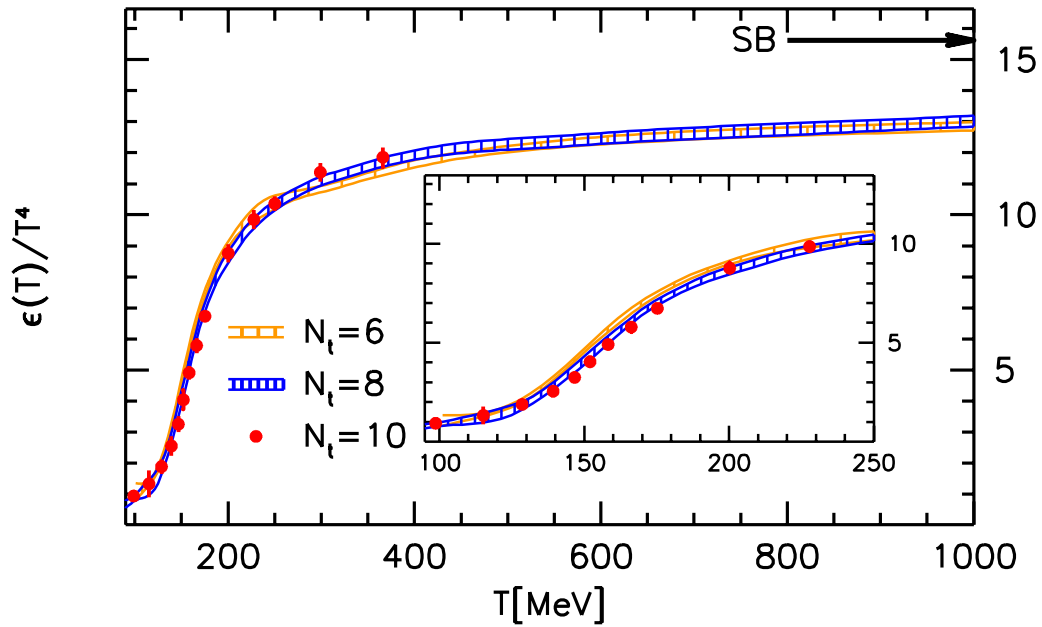


**Figure 11:** The energy density normalized by  $T^4$  as a function of the temperature on  $N_t = 6, 8$  and 10 lattices. The Stefan-Boltzmann limit  $\epsilon_{SB} = 3p_{SB}$  is indicated by an arrow.

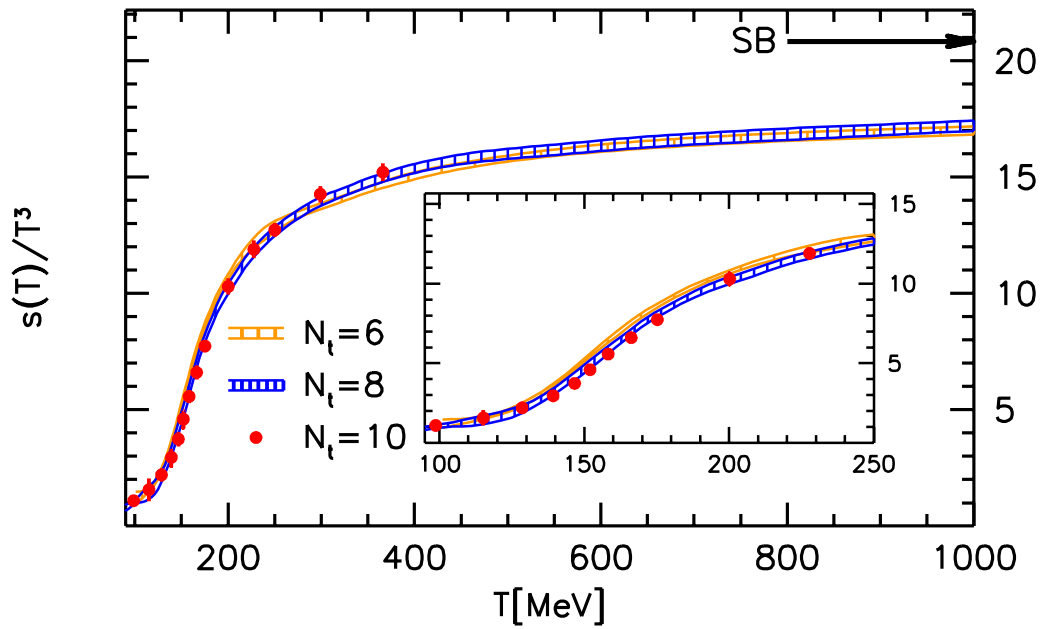


**Figure 12:** The entropy density normalized by  $T^3$  as a function of the temperature on  $N_t = 6, 8$  and 10 lattices. The Stefan-Boltzmann limit  $s_{SB} = 4p_{SB}/T$  is indicated by an arrow.

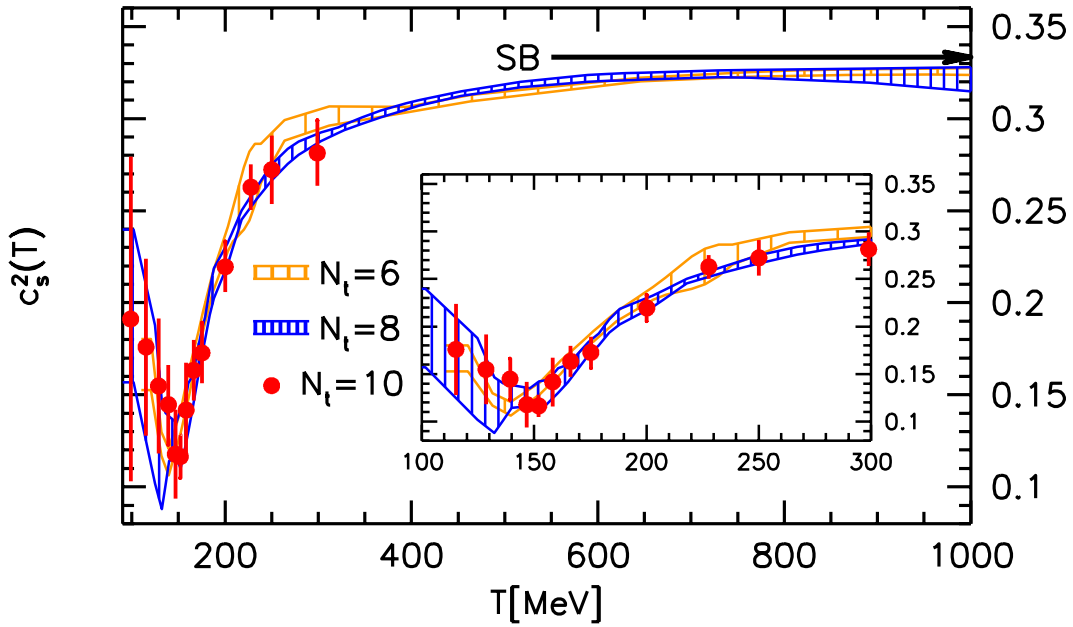


**Figure 13:** The squared of the speed of sound as a function of the temperature on  $N_t = 6, 8$  and  $10$  lattices. The Stefan-Boltzmann limit is  $c_{s,SB}^2 = 1/3$  indicated by an arrow.

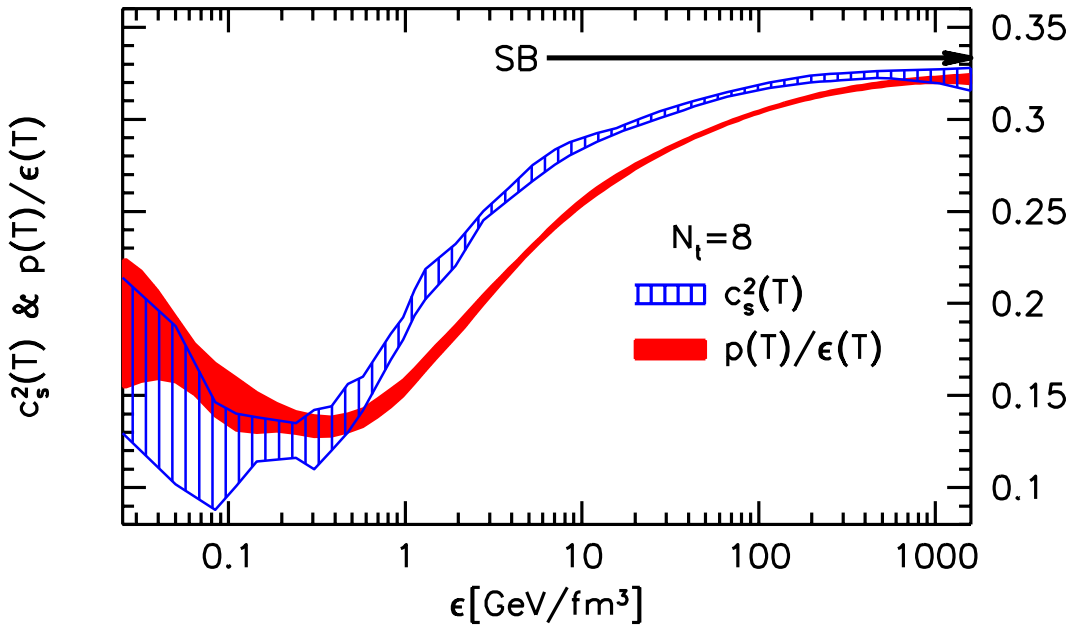


**Figure 14:** The speed of sound and  $p/\epsilon$  as a function of the energy density on  $N_t = 8$  lattices. The Stefan-Boltzmann limit is indicated by an arrow.

$n_f$	$h_0$	$h_1$	$h_2$	$f_0$	$f_1$	$f_2$	$g_1$	$g_2$
2 + 1	0.1396	-0.1800	0.0350	2.76	6.79	-5.29	-0.47	1.04
2 + 1 + 1				5.59	7.34	-5.60	1.42	0.50

**Table 2:** Parameters of the function in Equation (3.1) describing the trace anomaly in the  $n_f = 2 + 1$  and in the  $n_f = 2 + 1 + 1$  flavor cases.

For the reader’s convenience we also give a global parametrization of the trace anomaly as a function of the temperature. We took the following fit function:

$$\frac{I(T)}{T^4} = \exp(-h_1/t - h_2/t^2) \cdot \left( h_0 + \frac{f_0 \cdot [\tanh(f_1 \cdot t + f_2) + 1]}{1 + g_1 \cdot t + g_2 \cdot t^2} \right), \quad (3.1)$$

where the dimensionless  $t$  variable is defined as  $t = T/(200\text{MeV})$ . The parameters can be found in Table 2. This function reproduces the continuum estimate for the normalized trace anomaly in the entire temperature range  $T = 100 \dots 1000$  MeV. The  $\{f_0, f_1, f_2\}$  parameters describe the steep rise of the trace anomaly in the transition region, whereas the  $\{g_1, g_2\}$  parametrize the decrease for higher temperatures. The parametrization also approximates the HRG model prediction for  $T < 100$  MeV, this is described by the  $\{h_0, h_1, h_2\}$  parameters. For these temperatures the difference in the trace anomaly between the parametrization and the HRG model is less than  $\Delta(I(T)/T^4) \leq 0.07$ . From this parametrization the normalized pressure can be obtained by the definite integral

$$\frac{p(T)}{T^4} = \int_0^T \frac{dT}{T} \frac{I(T)}{T^4}. \quad (3.2)$$

The so obtained function goes through the points of the continuum estimate of the pressure for temperatures  $T = 100 \dots 1000$  MeV and for  $T < 100$  MeV the deviation from the HRG prediction is less than  $\Delta(p(T)/T^4) \leq 0.02$ . The parametrization together with our continuum estimate is shown on Figure 15.

### Light quark mass dependence

On Figure 16, the trace anomaly for two different values of the light quark masses is plotted: for the physical case, where  $m_{ud} = m_{ud}^{\text{phys}}$  and for the three degenerate flavor case, where  $m_{ud} = m_s^{\text{phys}}$ . This latter case corresponds to a pion mass of approximately  $m_\pi \sim 720$  MeV. The results are from our  $N_t = 8$  lattices, this is the smallest lattice spacing, where we have the complete mass dependence of the equation of state. As it is expected, the peak position of the trace anomaly is shifted towards higher temperature values for larger quark masses. The position in the three degenerate flavor case is  $\sim 25\%$  larger than at the physical point. The height also increases by about  $\sim 40\%$ . When zooming into the transition region, we also show the comparison with the HRG model. For low temperatures one finds a reasonable agreement also in the heavy quark mass case. As it is expected, the dependence on the quark masses vanishes as one goes to higher temperatures. Therefore it sounds plausible to compare the result with that of the massless perturbation theory. A good agreement can be observed with the highest order perturbative calculation without nonperturbative input ( $O(g^5)$ , see Figure 16).

In Appendix B we tabulate the  $N_t = 8$  pressure and trace anomaly for six different values of the quark mass ratio  $R$ .

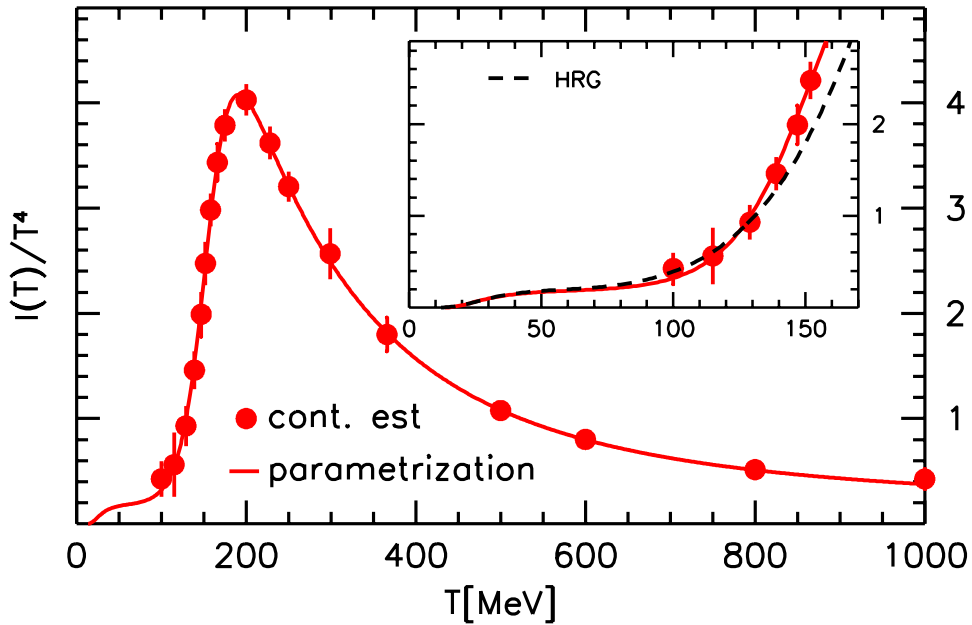


**Figure 15:** Continuum estimate for the trace anomaly normalized by  $T^4$  together with the parametrization of Equation (3.1) using the  $n_f = 2 + 1$  parameters from Table 2.

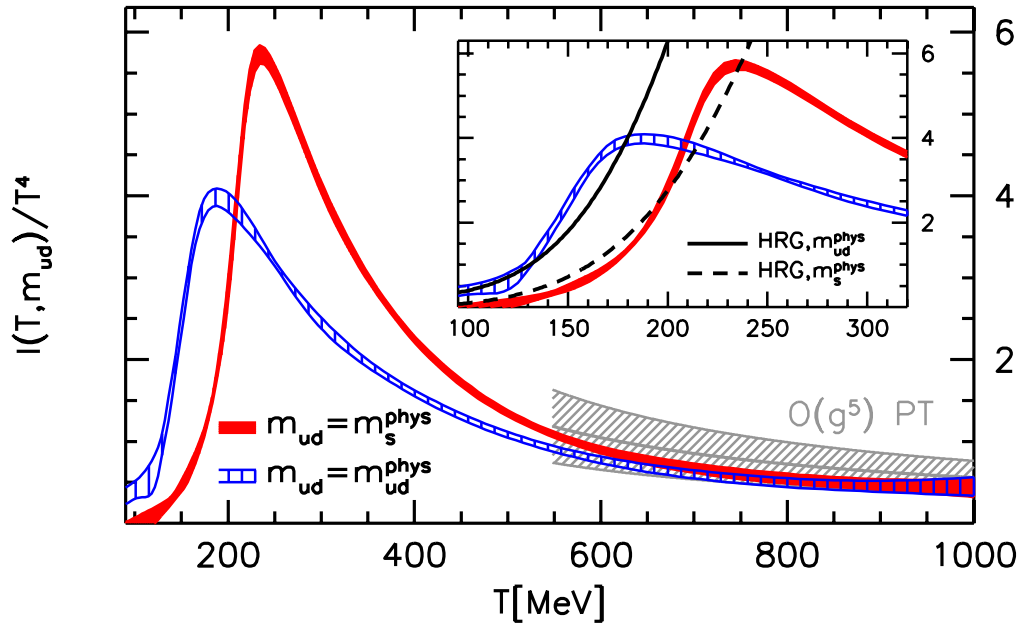


**Figure 16:** The normalized trace anomaly for two different values of the light quark masses on  $N_t = 8$  lattices: the physical  $m_{ud} = m_{ud}^{\text{phys}}$  and the three degenerate flavor  $m_{ud} = m_s^{\text{phys}}$  case.

### Estimate for the $n_f = 2 + 1 + 1$ flavor equation of state

While at low temperatures the equation of state only contains terms that originate from the light quarks, in high energy processes charm quarks can also be created from the vacuum, and they can also be present in the initial or final states. One expects that the charm quark plays an important role already above  $T \gtrsim 2 \cdot T_c$  [16]. The inclusion of its contribution is thus essential to determine the equation of state even in the temperature range covered by our work. We estimated the contribution of the charm quark on our  $N_t = 8$  lattices at several values of the charm to strange quark mass ratio  $Q$ . According to a recent high-precision lattice calculation [36] the physical value of  $Q$  is  $Q^{\text{phys}} = 11.85(16)$ . For this central value we show the contribution as a function of temperature on the upper part of Figure 17. It is non-zero already at temperatures  $T \sim 200$  MeV. The total  $n_f = 2 + 1 + 1$  pressure is compared to the already presented  $n_f = 2 + 1$  pressure on the lower panel of Figure 17. Let us emphasize here again, that the estimate for the charm contribution presented here suffers from two uncertainties: we neglected the back-reaction of the charm quarks on the gauge field, moreover due to the large mass of the charm large lattice artefacts are expected.

Using the parametrization in Equation (3.1) we fit the  $n_f = 2 + 1 + 1$  data at the  $N_t = 8$  lattice spacing, the fit parameters can be found in Table 2. We tabulated the charm contribution together with results for four other values of  $Q$  in Appendix B. From these, one also sees that the uncertainty in the lattice determination of  $Q^{\text{phys}}$  has no significant impact on the results.

### Comparison with different fermion discretizations

As it was already discussed in Reference [22], there is a disagreement between the results of current large scale thermodynamical calculations. The main difference can be described by a  $\sim 20$ -30 MeV shift in the temperature. This means, that the transition temperatures are different: the temperature values that we obtain are smaller by this amount than the values of the “hotQCD” collaboration. References [19] and [21] presented a possible explanation for this problem: the more severe discretization artefacts of the “asqtad” and “p4fat” actions used by the “hotQCD” collaboration lead to larger transition temperatures.

It is interesting to look for this discrepancy in the equation of state as well. On Figure 18 we compare the trace anomaly obtained in this study with the trace anomaly of the “hotQCD” collaboration. We plot the  $N_t = 8$  data using the “p4fat” and “asqtad” actions, which we took from References [13] and [14]. As it can be clearly seen, the upward going branch and the peak position are located at  $\sim 20$  MeV higher temperatures in the simulations of the “hotQCD” group. This is the same phenomenon as the one, which was already reported for many other quantities in Reference [22]. We also see, that the peak height is about 50% larger in the “hotQCD” case.

## 4. Conclusions, outlook

In this paper we determined the equation of state of QCD by means of lattice simulations. Results for the  $n_f = 2 + 1$  flavor pressure, trace anomaly, energy and entropy densities and for the speed of sound were presented on figures and in tables. We gave a simple parametrization for the trace anomaly. Moreover, the light quark mass dependence of the equation of state was investigated quantitatively. We also addressed the  $n_f = 2 + 1 + 1$

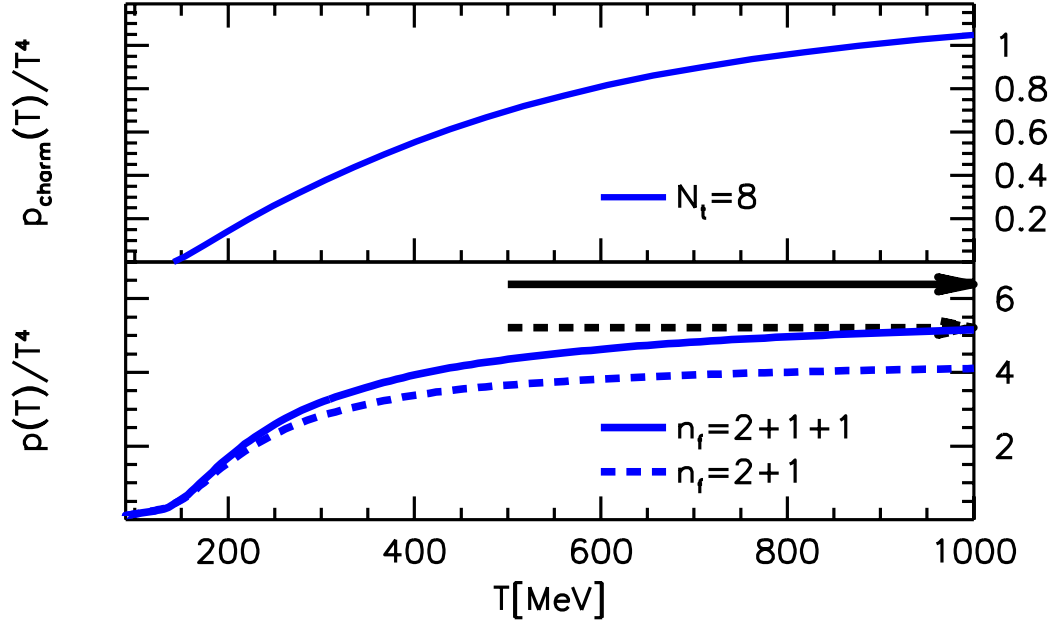


**Figure 17:** Upper figure: Contribution of the charm quark to the pressure on the  $N_t = 8$  lattices. Lower figure: The pressure normalized by  $T^4$  for  $n_f = 2 + 1 + 1$  and  $n_f = 2 + 1$  flavors on  $N_t = 8$  lattices. The corresponding Stefan-Boltzmann limits are indicated by arrows. The charm to strange quark mass ratio is  $Q = 11.85$  on this plot.

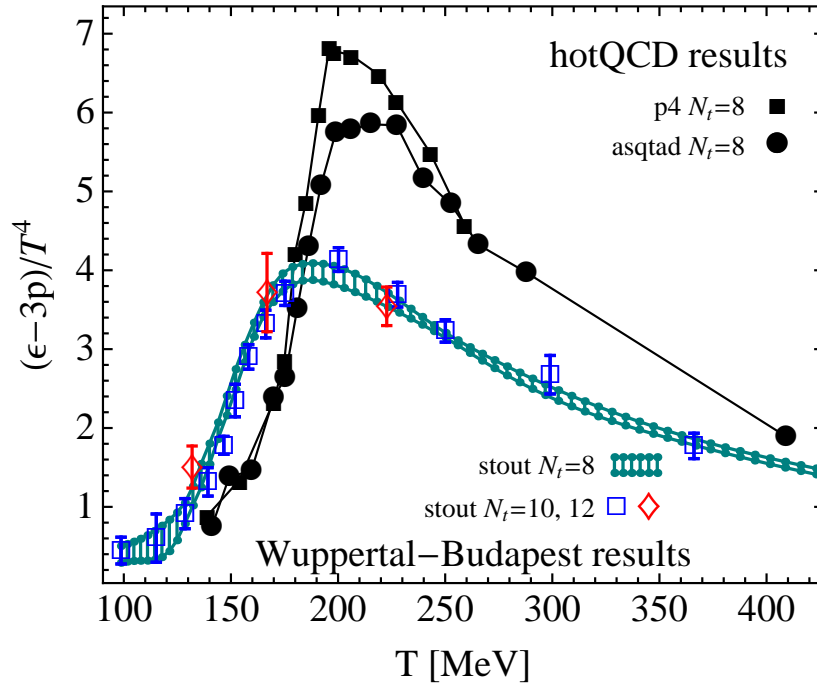


**Figure 18:** The normalized trace anomaly obtained in our study is compared to recent results from the “hotQCD” collaboration [13, 14].

flavor equation of state: an estimate of the charm quark contribution to the thermodynamic potential at the partially quenched level was given and a non-negligible effect down to temperatures of  $T \sim 200$  MeV was found.

The results were obtained by carrying out lattice simulations at four different lattice spacings  $N_t = 6, 8, 10$  and  $12$  in the temperature range  $T = 100 \dots 1000$  MeV. We developed and tested a new method to obtain the Lines of Constant Physics for these high temperature values. We also proposed a new method to get the pressure from quantities measured on the lattice: instead of the standard numerical integration procedure we fit a many parameter function to the lattice data. In order to reduce the lattice artefacts we applied tree-level improvement for all of the thermodynamical observables. We found that there is no difference in the results at the three finest lattice spacings. This shows that the lattice discretization errors are not significant and the continuum limit can be reliably taken. For low temperatures however, the apparent absence of the discretization artefacts might be misleading. Using the Hadron Resonance Gas model we estimated the discretization error of the lattice results for low temperatures. We ruled out the existence of significant finite size effects by comparing our results to a data set with double linear box size.

A comparison with the results of the “hotQCD” collaboration was made. The already reported problem, ie. the “hotQCD” results tend to give  $20 - 30$  MeV larger temperature values, is also present in the equation of state. Additionally we found that the peak of the trace anomaly is about 50% larger in the “hotQCD” calculations.

In order to provide a more precise calculation of the  $n_f = 2 + 1 + 1$  flavor equation of state, there is still room for improvements. First, one has to relax the uncontrolled partial quenched approximation and introduce the charm quark dynamically. Then, the lattice spacing has to be further reduced to ensure a good resolution of the charmed excitations. Finally, improved fermion actions are increasingly important when studying heavy quark degrees of freedom. A further obvious direction of improvement of the present work is to abandon the uncontrolled “rooting” issue of the staggered discretization and solve the same problem with e.g. Wilson-Clover fermions.

## Acknowledgments

Computations were performed on the Blue Gene supercomputers at FZ Jülich and on clusters at Wuppertal and also at the Eötvös University, Budapest. This work is supported in part by European Union (EU) grant I3HP; Deutsche Forschungsgemeinschaft grants FO 502/2 and SFB-TR 55 and (FP7/2007-2013)/ERC no. 208740, and by the U.S. Department of Energy under Grant No. DE-FG02-05ER25681.

## References

- [1] Y. Aoki, G. Endrodi, Z. Fodor, S. D. Katz, and K. K. Szabo, *The order of the quantum chromodynamics transition predicted by the standard model of particle physics*, Nature **443** (2006) 675–678, [[hep-lat/0611014](#)].
- [2] D. Teaney, J. Lauret, and E. V. Shuryak, *Flow at the SPS and RHIC as a quark gluon plasma signature*, Phys. Rev. Lett. **86** (2001) 4783–4786, [[nucl-th/0011058](#)].
- [3] D. Teaney, J. Lauret, and E. V. Shuryak, *A hydrodynamic description of heavy ion collisions at the SPS and RHIC*, [nucl-th/0110037](#).



- [4] P. F. Kolb and U. W. Heinz, *Hydrodynamic description of ultrarelativistic heavy-ion collisions*, [nucl-th/0305084](#).
- [5] G. Boyd et. al., *Thermodynamics of  $SU(3)$  Lattice Gauge Theory*, [Nucl. Phys.](#) **B469** (1996) 419–444, [[hep-lat/9602007](#)].
- [6] **CP-PACS** Collaboration, M. Okamoto et. al., *Equation of state for pure  $SU(3)$  gauge theory with renormalization group improved action*, [Phys. Rev.](#) **D60** (1999) 094510, [[hep-lat/9905005](#)].
- [7] **MILC** Collaboration, C. W. Bernard et. al., *The equation of state for two flavor QCD at  $N(t) = 6$* , [Phys. Rev.](#) **D55** (1997) 6861–6869, [[hep-lat/9612025](#)].
- [8] **CP-PACS** Collaboration, A. Ali Khan et. al., *Equation of state in finite-temperature QCD with two flavors of improved Wilson quarks*, [Phys. Rev.](#) **D64** (2001) 074510, [[hep-lat/0103028](#)].
- [9] F. Karsch, E. Laermann, and A. Peikert, *The pressure in 2, 2+1 and 3 flavour QCD*, [Phys. Lett.](#) **B478** (2000) 447–455, [[hep-lat/0002003](#)].
- [10] K. Kanaya et. al., *Towards the equation of state in 2+1 flavor QCD with improved Wilson quarks in the fixed scale approach*, [arXiv:0910.5284](#).
- [11] C. Bernard et. al., *QCD equation of state with 2+1 flavors of improved staggered quarks*, [Phys. Rev.](#) **D75** (2007) 094505, [[hep-lat/0611031](#)].
- [12] M. Cheng et. al., *The QCD Equation of State with almost Physical Quark Masses*, [Phys. Rev.](#) **D77** (2008) 014511, [[arXiv:0710.0354](#)].
- [13] A. Bazavov et. al., *Equation of state and QCD transition at finite temperature*, [Phys. Rev.](#) **D80** (2009) 014504, [[arXiv:0903.4379](#)].
- [14] M. Cheng et. al., *Equation of State for physical quark masses*, [Phys. Rev.](#) **D81** (2010) 054504, [[arXiv:0911.2215](#)].
- [15] Y. Aoki, Z. Fodor, S. D. Katz, and K. K. Szabo, *The equation of state in lattice QCD: With physical quark masses towards the continuum limit*, [JHEP](#) **01** (2006) 089, [[hep-lat/0510084](#)].
- [16] M. Laine and Y. Schroder, *Quark mass thresholds in QCD thermodynamics*, [Phys. Rev.](#) **D73** (2006) 085009, [[hep-ph/0603048](#)].
- [17] **RBC-Bielefeld** Collaboration, M. Cheng, *Charm Quarks and the QCD Equation of State*, [PoS LAT2007](#) (2007) 173, [[arXiv:0710.4357](#)].
- [18] L. Levkova, *Effects of the charm quark on the QCD equation of state*, [arXiv:0910.3006](#).
- [19] P. Huovinen and P. Petreczky, *QCD Equation of State and Hadron Resonance Gas*, [Nucl. Phys.](#) **A837** (2010) 26–53, [[arXiv:0912.2541](#)].
- [20] P. Huovinen and P. Petreczky, *On Fluctuations of Conserved Charges : Lattice Results Versus Hadron Resonance Gas*, [arXiv:1005.0324](#).
- [21] **Wuppertal-Budapest** Collaboration, S. Borsanyi et. al., *Is there still any  $T_c$  mystery in lattice QCD? Results with physical masses in the continuum limit III*, [arXiv:1005.3508](#).
- [22] Y. Aoki et. al., *The QCD transition temperature: results with physical masses in the continuum limit II*, [JHEP](#) **06** (2009) 088, [[arXiv:0903.4155](#)].
- [23] **HotQCD** Collaboration, A. Bazavov and P. Petreczky, *First results on QCD thermodynamics with HISQ action*, [PoS LAT2009](#) (2009) 163, [[arXiv:0912.5421](#)].
- [24] A. Bazavov and P. Petreczky, *Deconfinement and chiral transition with the highly improved staggered quark (HISQ) action*, [arXiv:1005.1131](#).

- [25] C. Morningstar and M. J. Peardon, *Analytic smearing of  $SU(3)$  link variables in lattice QCD*, Phys. Rev. **D69** (2004) 054501, [[hep-lat/0311018](#)].
- [26] Y. Aoki, Z. Fodor, S. D. Katz, and K. K. Szabo, *The QCD transition temperature: Results with physical masses in the continuum limit*, Phys. Lett. **B643** (2006) 46–54, [[hep-lat/0609068](#)].
- [27] S. Durr, *Theoretical issues with staggered fermion simulations*, PoS LAT2005 (2006) 021, [[hep-lat/0509026](#)].
- [28] S. Schaefer, R. Sommer, and F. Virotta, *Investigating the critical slowing down of QCD simulations*, [arXiv:0910.1465](#).
- [29] N. Ishizuka, M. Fukugita, H. Mino, M. Okawa, and A. Ukawa, *Operator dependence of hadron masses for Kogut-Susskind quarks on the lattice*, Nucl. Phys. **B411** (1994) 875–902.
- [30] **Particle Data Group** Collaboration, C. Amsler *et. al.*, *Review of particle physics*, Phys. Lett. **B667** (2008) 1.
- [31] M. Luscher, P. Weisz, and U. Wolff, *A Numerical method to compute the running coupling in asymptotically free theories*, Nucl. Phys. **B359** (1991) 221–243.
- [32] E. Bilgici *et. al.*, *A new scheme for the running coupling constant in gauge theories using Wilson loops*, Phys. Rev. **D80** (2009) 034507, [[arXiv:0902.3768](#)].
- [33] **APE** Collaboration, M. Albanese *et. al.*, *Glueball Masses and String Tension in Lattice QCD*, Phys. Lett. **B192** (1987) 163.
- [34] S. Necco and R. Sommer, *The  $N(f) = 0$  heavy quark potential from short to intermediate distances*, Nucl. Phys. **B622** (2002) 328–346, [[hep-lat/0108008](#)].
- [35] M. Gockeler *et. al.*, *A determination of the Lambda parameter from full lattice QCD*, Phys. Rev. **D73** (2006) 014513, [[hep-ph/0502212](#)].
- [36] C. T. H. Davies *et. al.*, *Precise Charm to Strange Mass Ratio and Light Quark Masses from Full Lattice QCD*, Phys. Rev. Lett. **104** (2010) 132003, [[arXiv:0910.3102](#)].
- [37] J. Engels, J. Fingberg, F. Karsch, D. Miller, and M. Weber, *Nonperturbative thermodynamics of  $SU(N)$  gauge theories*, Phys. Lett. **B252** (1990) 625–630.
- [38] G. Endrodi, *Multidimensional spline integration of scattered data*, [arXiv:1010.2952](#).
- [39] F. Karsch, K. Redlich, and A. Tawfik, *Hadron resonance mass spectrum and lattice QCD thermodynamics*, Eur. Phys. J. **C29** (2003) 549–556, [[hep-ph/0303108](#)].
- [40] F. Karsch, K. Redlich, and A. Tawfik, *Thermodynamics at non-zero baryon number density: A comparison of lattice and hadron resonance gas model calculations*, Phys. Lett. **B571** (2003) 67–74, [[hep-ph/0306208](#)].
- [41] A. Tawfik, *The QCD phase diagram: A comparison of lattice and hadron resonance gas model calculations*, Phys. Rev. **D71** (2005) 054502, [[hep-ph/0412336](#)].
- [42] J. Gasser and H. Leutwyler, *Chiral Perturbation Theory to One Loop*, Ann. Phys. **158** (1984) 142.
- [43] R. Dashen, S.-K. Ma, and H. J. Bernstein, *S Matrix formulation of statistical mechanics*, Phys. Rev. **187** (1969) 345–370.
- [44] R. Venugopalan and M. Prakash, *Thermal properties of interacting hadrons*, Nucl. Phys. **A546** (1992) 718–760.
- [45] J. Noronha-Hostler, C. Greiner, and I. A. Shovkovy, *Fast Equilibration of Hadrons in an Expanding Fireball*, Phys. Rev. Lett. **100** (2008) 252301, [[arXiv:0711.0930](#)].

[46] J. Noronha-Hostler, M. Beitel, C. Greiner, and I. Shovkovy, *Dynamics of Chemical Equilibrium of Hadronic Matter Close to  $T_c$* , Phys. Rev. **C81** (2010) 054909, [arXiv:0909.2908].

[47] A. Majumder and B. Muller, *Hadron Mass Spectrum from Lattice QCD*, arXiv:1008.1747.

## A. The pressure from a 2D spline fit

In this Appendix we describe the method, which was used to obtain the pressure as a function of the parameters  $\beta$  and  $R$  using its measured derivatives (Equations (2.14) and (2.15)). Further details can be found in Reference [38].

Let us first construct a two dimensional bicubic spline function  $P(\beta, R)$ . We start from a grid of node points  $\{\beta_k, R_l\}$  with  $0 \leq k < K$  and  $0 \leq l < L$ . Upon this grid  $P(\beta, R)$  is unambiguously determined by the values  $p_{kl}$  that it takes at these node points. The spline coefficients can be written compactly as  $C_{ab,kl}$  with  $0 \leq a < 4$  and  $0 \leq b < 4$  being the indices for the appropriate powers of  $\beta$  and  $R$ , and  $k$  and  $l$  indicate the corresponding grid square  $[\beta_k, \beta_{k+1}] \times [R_l, R_{l+1}]$ . There are  $16 \cdot (K - 1) \cdot (L - 1)$  coefficients altogether. The spline function  $P$  and its first and second derivatives are continuous along the grid lines  $\{\beta_k, \cdot\}$  and  $\{\cdot, R_l\}$ , and the second derivatives go to zero at the two ends. These constraints and the condition

$$P(\beta_k, R_l) = p_{kl} \quad (\text{A.1})$$

constitute a linear system of equations for  $C_{ab,kl}$ , that can be solved to give

$$C_{ab,kl} = \sum_{k'=0}^{K-1} \sum_{l'=0}^{L-1} X_{ab,kl;k'l'} p_{k'l'} \quad (\text{A.2})$$

with  $X$  being a matrix of size  $16 \cdot (K - 1) \cdot (L - 1) \times K \cdot L$ .

Next we determine the spline coefficients by fitting the derivatives of the  $P(\beta, R)$  function to the measured derivatives  $D_\beta$  and  $D_R$  in Equations (2.14) and (2.15). Since the two derivatives are determined using the same configurations at a given value of the bare parameters, their correlation has to be taken into account in the  $\chi^2$  fitting. The  $\chi^2$  function will be a quadratic function of the values  $p_{kl}$  and therefore it can be minimized by solving a  $K \cdot L$  dimensional system of linear equations:

$$\sum_{k'=0}^{K-1} \sum_{l'=0}^{L-1} M_{kl,k'l'} p_{k'l'} = V_{kl}. \quad (\text{A.3})$$

Here the matrix  $M$  and the vector  $V$  can be calculated using the matrix  $X$  and the values of the measured derivatives  $D_\beta$  and  $D_R$ . The system of linear equations in Equation (A.3) can be solved for  $p_{kl}$  and with it the spline coefficients are also determined through Equation (A.2). These unambiguously determine the whole pressure surface  $P(\beta, R)$ . The solution is of course indeterminate up to an overall constant, which does not influence the gradient of the surface.

The coordinates of the node points in the  $R$ -direction were set to be halfway between the measurement points ranging from  $R_l = 1.0 \dots 28.15$  in order to ensure the stability of the fit. The coordinates in the  $\beta$ -direction on the other hand were varied randomly around a “stable” fit to estimate the systematic error of this fitting procedure. The number of

node points were also varied. This analysis shows that for the pressure the systematic error related to our integration procedure is around or less than the statistical one. For the trace anomaly, this error is larger for some temperature values. We added the statistical and systematic errors in quadrature.

## B. Tables

$p(T)/T^4$						
T[MeV]	$m_\pi$ [MeV]					
	716	414	271	191	160	135
100	<b>0</b>	0.05(1)	0.10(1)	0.13(1)	0.14(1)	0.16(1)
115	-0.02(3)	0.03(6)	0.13(4)	0.14(6)	0.23(6)	0.23(5)
129	0.02(4)	0.11(4)	0.19(4)	0.25(4)	0.28(4)	0.30(4)
134	0.03(4)	0.12(4)	0.22(4)	0.29(4)	0.32(4)	0.34(4)
139	0.04(4)	0.15(4)	0.25(4)	0.33(4)	0.37(4)	0.40(4)
143	0.04(4)	0.17(4)	0.30(4)	0.38(4)	0.42(4)	0.45(4)
147	0.05(4)	0.20(4)	0.34(4)	0.43(4)	0.47(4)	0.51(4)
152	0.07(4)	0.24(4)	0.39(4)	0.50(4)	0.54(4)	0.58(4)
158	0.09(4)	0.30(4)	0.48(5)	0.59(5)	0.64(5)	0.68(5)
162	0.11(4)	0.34(4)	0.53(5)	0.67(5)	0.72(5)	0.76(5)
166	0.13(4)	0.39(5)	0.60(4)	0.75(4)	0.80(4)	0.85(4)
170	0.15(5)	0.43(5)	0.68(5)	0.84(5)	0.90(5)	0.94(5)
175	0.18(5)	0.51(5)	0.80(5)	0.95(4)	1.01(5)	1.05(5)
185	0.25(5)	0.72(5)	1.03(4)	1.19(4)	1.24(4)	1.27(4)
200	0.43(5)	1.06(5)	1.38(5)	1.51(5)	1.54(5)	1.57(5)
215	0.68(5)	1.43(5)	1.70(4)	1.80(5)	1.83(5)	1.85(5)
228	0.98(4)	1.72(5)	1.95(5)	2.03(5)	2.05(5)	2.06(5)
250	1.51(5)	2.13(5)	2.29(5)	2.35(5)	2.36(5)	2.37(5)
275	2.00(4)	2.49(5)	2.61(5)	2.64(5)	2.65(5)	2.66(5)
299	2.39(5)	2.75(5)	2.84(5)	2.87(5)	2.87(5)	2.87(5)
330	2.74(4)	3.00(4)	3.06(5)	3.08(5)	3.08(5)	3.08(5)
366	3.06(5)	3.24(5)	3.28(5)	3.29(5)	3.29(5)	3.29(5)
400	3.28(5)	3.42(5)	3.44(5)	3.44(5)	3.45(5)	3.45(5)
450	3.52(5)	3.60(5)	3.61(5)	3.61(5)	3.62(5)	3.62(5)
500	3.67(5)	3.73(5)	3.73(5)	3.73(5)	3.73(5)	3.73(5)
600	3.87(5)	3.89(5)	3.89(5)	3.88(6)	3.90(5)	3.90(5)
800	4.08(6)	4.09(6)	4.09(6)	4.09(6)	4.09(6)	4.09(6)
1000	4.19(6)	4.19(6)	4.19(6)	4.19(6)	4.19(6)	4.19(6)

**Table 3:**  $N_t = 8$  results for the normalized pressure  $p(T)/T^4$  at different pion masses described by the quark mass ratio  $R = m_g^{\text{phys}}/m_{ud}$ . The pion masses correspond to  $R = 1, 3, 7, 14, 20$  and 28.15. The zero point of the pressure was set at  $R = 1, T = 100$  MeV.

$I(T)/T^4$						
T[MeV]	$m_\pi$ [MeV]					
	716	414	271	191	160	135
100	-0.04(11)	0.26(09)	0.41(07)	0.35(09)	0.37(10)	0.41(11)
115	0.05(11)	0.41(10)	0.63(08)	0.38(16)	0.47(18)	0.52(19)
129	0.17(07)	0.57(08)	0.88(09)	0.80(11)	0.91(12)	0.95(13)
134	0.22(06)	0.64(07)	0.98(09)	1.11(11)	1.22(11)	1.25(13)
139	0.28(05)	0.74(06)	1.13(09)	1.39(13)	1.54(13)	1.60(14)
143	0.34(05)	0.84(06)	1.29(09)	1.60(11)	1.80(11)	1.89(11)
147	0.40(06)	1.00(07)	1.50(09)	1.86(12)	2.08(12)	2.20(12)
152	0.49(08)	1.26(08)	1.85(09)	2.28(12)	2.49(13)	2.60(13)
158	0.62(08)	1.66(09)	2.35(09)	2.87(10)	2.99(10)	3.06(10)
162	0.72(08)	1.97(09)	2.69(09)	3.23(09)	3.29(09)	3.33(09)
166	0.83(07)	2.30(09)	3.04(10)	3.55(09)	3.55(11)	3.55(09)
170	0.96(06)	2.65(09)	3.37(10)	3.80(10)	3.75(12)	3.72(11)
175	1.14(05)	3.10(08)	3.75(10)	4.01(11)	3.92(13)	3.87(11)
185	1.62(05)	3.97(08)	4.32(09)	4.18(10)	4.06(12)	3.98(10)
200	2.83(14)	4.90(13)	4.64(13)	4.12(12)	4.00(13)	3.92(12)
215	4.65(13)	5.06(12)	4.33(11)	3.93(10)	3.81(12)	3.75(11)
228	5.63(13)	4.76(10)	3.96(09)	3.71(08)	3.60(08)	3.55(08)
250	5.51(09)	4.08(06)	3.52(06)	3.31(03)	3.22(03)	3.18(03)
275	4.82(07)	3.44(06)	3.03(05)	2.87(05)	2.80(05)	2.78(05)
299	4.13(07)	2.96(07)	2.62(06)	2.51(06)	2.47(06)	2.46(07)
330	3.40(06)	2.49(06)	2.22(06)	2.15(05)	2.14(06)	2.13(06)
366	2.73(04)	2.07(04)	1.88(04)	1.82(04)	1.83(04)	1.82(04)
400	2.25(04)	1.75(03)	1.63(03)	1.58(04)	1.60(04)	1.59(04)
450	1.72(04)	1.40(04)	1.33(04)	1.30(04)	1.31(04)	1.31(04)
500	1.35(04)	1.14(04)	1.10(04)	1.09(04)	1.08(04)	1.08(04)
600	0.90(04)	0.80(04)	0.80(04)	0.80(05)	0.76(04)	0.77(04)
800	0.55(06)	0.51(05)	0.51(06)	0.52(06)	0.49(05)	0.50(05)
1000	0.43(11)	0.44(10)	0.43(11)	0.40(13)	0.48(12)	0.45(11)

**Table 4:**  $N_t = 8$  results for the normalized trace anomaly  $I(T)/T^4$  at different pion masses described by the quark mass ratio  $R = m_s^{\text{phys}}/m_{ud}$ . The pion masses correspond to  $R = 1, 3, 7, 14, 20$  and 28.15.

T[MeV]	$N_t = 6$			$N_t = 8$			$N_t = 10$			cont. estimate		
	$p/T^4$	$I/T^4$	$c_s^2$	$p/T^4$	$I/T^4$	$c_s^2$	$p/T^4$	$I/T^4$	$c_s^2$	$p/T^4$	$I/T^4$	$c_s^2$
100	0.12(0)	0.71(29)	0.19(9)	0.16(1)	0.41(11)	0.20(2)	0.16(4)	0.45(17)	0.19(9)	0.22(4)	0.43(17)	0.19(9)
115	0.21(0)	0.72(7)	0.19(2)	0.23(5)	0.52(19)	0.19(3)	0.24(6)	0.60(31)	0.18(5)	0.29(6)	0.56(31)	0.18(5)
129	0.32(1)	1.16(8)	0.13(0)	0.30(4)	0.95(13)	0.12(3)	0.32(6)	0.91(19)	0.15(4)	0.37(6)	0.93(19)	0.14(4)
139	0.42(1)	1.89(9)	0.11(0)	0.40(4)	1.60(14)	0.12(1)	0.41(6)	1.32(18)	0.14(2)	0.46(6)	1.46(18)	0.13(2)
147	0.54(1)	2.58(8)	0.12(0)	0.51(4)	2.20(12)	0.13(1)	0.49(7)	1.78(11)	0.12(2)	0.55(7)	1.99(21)	0.12(2)
152	0.63(2)	2.97(9)	0.13(0)	0.58(4)	2.60(13)	0.13(2)	0.56(7)	2.35(21)	0.12(1)	0.63(7)	2.47(21)	0.12(2)
158	0.75(2)	3.37(10)	0.15(1)	0.68(5)	3.06(10)	0.14(1)	0.67(7)	2.90(16)	0.14(3)	0.73(7)	2.98(16)	0.14(3)
166	0.94(2)	3.76(11)	0.17(0)	0.85(4)	3.55(9)	0.15(0)	0.82(7)	3.32(18)	0.16(2)	0.89(7)	3.43(18)	0.16(2)
175	1.15(2)	4.00(9)	0.19(0)	1.05(5)	3.87(11)	0.18(0)	1.01(6)	3.71(15)	0.17(2)	1.08(6)	3.79(15)	0.18(2)
200	1.69(2)	3.98(8)	0.23(0)	1.57(5)	3.92(12)	0.22(0)	1.54(6)	4.14(15)	0.22(1)	1.61(6)	4.03(15)	0.22(1)
228	2.18(2)	3.47(19)	0.27(2)	2.06(5)	3.55(8)	0.25(0)	2.05(7)	3.69(16)	0.26(1)	2.11(7)	3.62(16)	0.26(1)
250	2.48(2)	2.97(20)	0.29(0)	2.37(5)	3.18(3)	0.27(0)	2.38(7)	3.23(14)	0.27(2)	2.43(7)	3.20(14)	0.27(2)
299	2.92(3)	2.06(5)	0.30(0)	2.87(5)	2.46(7)	0.29(0)	2.90(7)	2.68(24)	0.28(2)	2.94(7)	2.57(24)	0.29(2)
366	3.28(3)	1.54(5)	0.30(0)	3.29(5)	1.82(4)	0.30(0)	3.36(8)	1.77(16)	0.33(3)	3.38(8)	1.80(16)	0.32(3)
500	3.68(3)	1.07(4)	0.31(0)	3.73(5)	1.08(4)	0.32(0)	-	-	-	3.76(5)	1.08(4)	0.32(0)
600	3.85(3)	0.83(5)	0.32(0)	3.90(5)	0.77(4)	0.32(0)	-	-	-	3.93(5)	0.80(5)	0.32(0)
800	4.05(4)	0.53(3)	0.32(0)	4.09(6)	0.50(5)	0.32(0)	-	-	-	4.12(6)	0.51(5)	0.32(0)
1000	4.15(4)	0.40(4)	0.33(0)	4.19(6)	0.45(11)	0.32(0)	-	-	-	4.23(6)	0.43(11)	0.32(0)

**Table 5:** Lattice data for the pressure, trace anomaly and the speed of sound as functions of the temperature. We also give a continuum estimate based on the mean of the finest two discretizations at a given temperature. In the continuum estimate of  $p/T^4$  there is an additional systematic uncertainty of 0.06, which is not included in the table.

$p_{\text{charm}}(T)/T^4$					
$T[\text{MeV}]$	$Q$				
	10.75	11.85	12.5	16.0	20.0
147	0.01(0)	0.01(0)	0.01(0)	0.01(0)	0.01(0)
152	0.02(0)	0.02(0)	0.02(0)	0.02(0)	0.01(0)
158	0.04(0)	0.04(0)	0.04(0)	0.03(0)	0.02(0)
162	0.05(0)	0.05(0)	0.05(0)	0.04(0)	0.03(0)
166	0.06(0)	0.06(0)	0.06(0)	0.04(0)	0.03(0)
170	0.07(0)	0.07(0)	0.07(0)	0.05(0)	0.04(0)
175	0.09(0)	0.08(0)	0.08(0)	0.06(0)	0.05(0)
185	0.12(0)	0.10(0)	0.10(0)	0.08(0)	0.06(0)
200	0.16(0)	0.14(0)	0.14(0)	0.11(0)	0.08(0)
215	0.20(0)	0.18(0)	0.18(0)	0.14(0)	0.10(0)
228	0.23(0)	0.21(0)	0.20(0)	0.16(0)	0.12(0)
250	0.28(0)	0.26(0)	0.25(1)	0.21(0)	0.15(0)
275	0.34(0)	0.32(1)	0.31(1)	0.25(0)	0.19(1)
299	0.39(0)	0.37(1)	0.35(1)	0.29(1)	0.22(1)
330	0.46(0)	0.43(1)	0.41(1)	0.34(1)	0.26(1)
366	0.53(1)	0.49(1)	0.48(1)	0.40(1)	0.31(2)
400	0.58(1)	0.55(1)	0.53(1)	0.45(1)	0.35(2)
450	0.66(1)	0.63(1)	0.61(1)	0.52(1)	0.41(2)
500	0.73(1)	0.70(1)	0.68(1)	0.58(1)	0.46(2)
600	0.84(1)	0.81(1)	0.79(1)	0.69(1)	0.56(1)
800	0.98(1)	0.96(1)	0.95(1)	0.86(0)	0.73(1)
1000	1.06(1)	1.05(1)	1.04(1)	0.97(0)	0.86(1)

**Table 6:**  $N_t = 8$  results for the charm contribution to the pressure  $p_{\text{charm}}(T)/T^4$  at different values of the quark mass ratio  $Q = m_c/m_s^{\text{phys}}$ . The value  $Q = 11.85$  corresponds to a recent charm mass determination [36]. Note, that there are additional systematic uncertainties related to the partial quenching approximation.